Aus dem Zentrum für Pharmakologie
der Universität zu Köln
Institut I für Pharmakologie
Direktor (beurlaubt): Universitätsprofessor Dr. med. E. Schömig
Kommissarischer Leiter: Universitätsprofessor Dr. med. U. Fuhr

High Expression of Neuronal Calcium Sensor 1 Induces an Invasive Cellular Phenotype and Predicts Poor Disease Outcome in a Subset of Cancer Patients

Inaugural-Dissertation zur Erlangung der Doktorwürde
der Medizinischen Fakultät
der Universität zu Köln

vorgelegt von
Daniel Schütte
aus Paderborn

promoviert am 14. März 2023

Gedruckt mit Genehmigung der Medizinischen Fakultät der Universität zu Köln
2022

Dekan: Universitätsprofessor Dr. med. G. R. Fink

1. Gutachterin oder Gutachter: Privatdozent Dr. med. J. Matthes
2. Gutachterin oder Gutachter: Universitätsprofessor Dr. med. T. Goeser
3. Gutachterin oder Gutachter: Universitätsprofessor Dr. med. B. von Tresckow

Erklärung

Ich erkläre hiermit, dass ich die vorliegende Dissertationsschrift ohne unzulässige Hilfe Dritter und ohne Benutzung anderer als der angegebenen Hilfsmittel angefertigt habe; die aus fremden Quellen direkt oder indirekt übernommenen Gedanken sind als solche kenntlich gemacht.[1]

Bei der Auswahl und Auswertung des Materials sowie bei der Herstellung des Manuskriptes habe ich keine Unterstützungsleistungen erhalten.

Weitere Personen waren an der Erstellung der vorliegenden Arbeit nicht beteiligt. Insbesondere habe ich nicht die Hilfe einer Promotionsberaterin/eines Promotionsberaters in Anspruch genommen. Dritte haben von mir weder unmittelbar noch mittelbar geldwerte Leistungen für Arbeiten erhalten, die im Zusammenhang mit dem Inhalt der vorgelegten Dissertationsschrift stehen.

Die Dissertationsschrift wurde von mir bisher weder im Inland noch im Ausland in gleicher oder ähnlicher Form einer anderen Prüfungsbehörde vorgelegt.

Im Folgenden wird mein Anteil an der Arbeit

Daniel Schuette, Lauren M. Moore, Marie E. Robert, Tamar H. Taddei, and Barbara E. Ehrlich: *Hepatocellular Carcinoma Outcome is Predicted by Expression of Neuronal Calcium Sensor 1*. Cancer Epidemiol Biomarkers Prev. Published May 2018. DOI: 10.1158/1055-9965.EPI-18-0167.

beschrieben:

Die dieser Arbeit zugrunde liegenden Datensätze wurden ohne meine Mitarbeit multizentrisch erhoben und sind öffentlich über Datenbanken des Forschungsnetzwerks „The Cancer Genome Atlas“, das „International Cancer Genome Consortium“, die „Cancer Cell Line Encyclopedia“, das „Genotype-Tissue Expression Project“ und den „Human Protein Atlas“ abrufbar. Der Download aller genomischen Daten, die Anlage einer SQL Datenbank zur effizienten Abfrage sowie die statistische Analyse und Aufarbeitung hat unter Verwendung der Programmiersprachen „R“, „Python“ und „Go“ durch mich stattgefunden.

Die automatische, Bias-freie Korrelation von Gen-Expressionswerten und molekularen Signalwegen ist von mir durchgeführt worden, hierzu kamen die genannten Programmiersprachen, die „Exploratory Gene Association Networks“ Software sowie die „Molecular Signature Database“ des Broad Institute zur Anwendung.

Die pathologische Begutachtung der Leberkrebs-Microarrays mittels Immunohistochemie erfolgte durch Frau Lauren M. Moore, die statistische Analyse fand durch mich statt.

Die der Arbeit zugrunde liegende Forschungsfragestellung wurde in Kollaboration aller Ko-Autoren erarbeitet. Das Design und die Ausführung der Computerexperimente erfolgte durch mich. Das erste Manuskript der Publikation sowie die Abbildungen wurden durch mich erstellt, die detaillierte Revision des Manuskripts fand durch alle Ko-Autoren statt.

Im Folgenden wird mein Anteil an der Arbeit

Jonathan E. Apasu, **Daniel Schuette**, Ryan LaRanger, Julia A. Steinle, Lien D. Nguyen, Henrike K. Grosshans, Meiling Zhang, Wesley L. Cai, Qin Yan, Marie E. Robert, Michael Mak, and Barbara E. Ehrlich: *Neuronal calcium sensor 1 (NCS1) promotes motility and metastatic spread of breast cancer cells in vitro and in vivo*. FASEB J. Published April 2019. DOI: 10.1096/fj.201802004R.

beschrieben:

Die in dieser Arbeit in Abbildung 1 dargestellten Zellproliferations-Assays sowie Westernblot -Experimente wurden von mir durchgeführt und validiert.

Die in Abbildung 2 gezeigten konfokalmikroskopischen Bilder wurden von Frau Lien D. Nguyen hergestellt und von mir zur Validierung repliziert.

Die in Abbildung 3 wiedergegebenen morphologischen und Zellmotilitäts-Datensätze wurden von Herrn Ryan LaRanger experimentell erhoben, das Design und die Auswertung der Experimente unter Nutzung der „Matlab“ Programmiersprache erfolgten in Zusammenarbeit mit mir.

Die in Abbildung 4 und 5 beschriebenen Mausexperimente inklusive der histopathologischen Begutachtung wurden von Herrn Jonathan E. Apasu und Frau Marie E. Robert durchgeführt, die Aufarbeitung und Analyse der Daten fand mithilfe der „Python“ Programmiersprache durch mich statt.

Die der Arbeit zugrunde liegende Forschungsfragestellung wurde in Kollaboration aller Ko-Autoren erarbeitet. Das erste Manuskript der Publikation sowie die Abbildungen wurden von mir erstellt, die detaillierte Revision des Manuskripts fand durch alle Ko-Autoren statt.

Erklärung zur guten wissenschaftlichen Praxis:

Ich erkläre hiermit, dass ich die Ordnung zur Sicherung guter wissenschaftlicher Praxis und zum Umgang mit wissenschaftlichem Fehlverhalten (Amtliche Mitteilung der Universität zu Köln AM 132/2020) der Universität zu Köln gelesen habe und verpflichte mich hiermit, die dort genannten Vorgaben bei allen wissenschaftlichen Tätigkeiten zu beachten und umzusetzen.

Köln, den 18.03.2022

Unterschrift: _____

[1]Bei kumulativen Promotionen stellt nur die eigenständig verfasste Einleitung und Diskussion die Dissertationsschrift im Sinne der Erklärung gemäß dieser Erklärung dar.

Danksagung

Mein herzlichster Dank gilt Frau Professor Barbara Ehrlich. Ihr herausragendes Mentoring hat diese Arbeit möglich und mein Forschungsjahr zu einem vollen Erfolg gemacht.
Ebenso möchte ich allen Mitgliedern des Yale Laboratory of Molecular Hermeneutics für die produktive Zusammenarbeit und die vielfältigen Hilfestellungen danken, die ich in den 12 Monaten meines Aufenthaltes in New Haven erfahren habe. Die Möglichkeit eines Forschungsaufenthaltes in den USA verdanke ich nicht zuletzt der Studienstiftung des deutschen Volkes, die mich finanziell sowie ideell gefördert hat. Für diese Begleitung über mein gesamtes Studium hinweg bin ich sehr dankbar.
Ein großes Dankeschön möchte ich Herrn PD Dr. Jan Matthes aussprechen, der sich trotz der Distanz zu meiner eigentlichen experimentellen Arbeit bereiterklärte, meine Forschung als Mitglied der medizinischen Fakultät aus Köln heraus zu betreuen und der mich stets mit Rat und Tat in meinem Promotionsvorhaben unterstützte.
Ein besonderer Dank gilt meinen Eltern, die mich in allen Phasen des Studiums und meiner wissenschaftlichen Tätigkeit gefördert und ermutigt haben.

Table of Contents

List of Abbreviations

ADCY: Adenylate Cyclase

ADORA2A: Adenosine A2 Receptor

ATP: Adenosine Triphosphate

BCR: B-Cell Receptor

Ca^{2+}: Calcium Ion

CALM: Calmodulin

cAMP: Cyclic Adenosine Monophosphate

CaSR: Calcium-Sensing Receptor

CaV1-3: Voltage Gated Calcium Channels (L-, N-, P-, R-, T-Types)

CCLE: Cancer Cell Line Encyclopedia

CDH-1: Cadherin 1

CIPN: Chemotherapy-Induced Peripheral Neuropathy

DAG: Diacylglycerol

EMT: Epithelial-to-Mesenchymal Transition

ER: Endoplasmic Reticulum

G_q: G-Protein

GPCR: G-Protein Coupled Receptor

GRK2: G-Protein Coupled Receptor Kinase 2

G_s: Stimulatory G-Protein

GTP: Guanosine Triphosphate

HCC: Hepatocellular Carcinoma

IHC: Immunohistochemistry

IL1RAPL: Interleukin-1 Receptor Accessory Protein-Like 1

IP_3: Inositol Triphosphate

IP_3R: Inositol Triphosphate Receptor

LIMK-1: LIM-Domain Kinase 1

MAPK: Mitogen-Activated Protein Kinase

MLCK: Myosin Light-Chain Kinase

MMP: Matrix Metalloproteinase

NCS-1: Neuronal Calcium Sensor 1

NFAT: Nuclear Factor of Activated T-Cells

OE: Overexpression

ORAI: Calcium Release-Activated Calcium Channel Protein

PIP_3: Phosphatidylinositol Trisphosphate

PI3K: Phosphoinositide-3-Kinase

PKB: Proteinkinase B (also known as AKT)

PKC: Proteinkinase C

PLC: Phospholipase C

Rac-1: Ras-Related C3 Botulinum Toxin Substrate 1

RhoA: Ras Homolog Family Member A

ROC: Receptor-Operated Calcium Channel

ROCK: RHO-Associated Protein Kinase

RTK: Receptor Tyrosine Kinase

RYR: Ryanodine Receptors

SERCA: Sarcoplasmic/Endoplasmic Reticulum Calcium ATPase

SOC: Store-Operated Calcium

TCGA: The Cancer Genome Atlas

TCR: T-Cell Receptor

TnC: Troponin C

TRP: Transient Receptor Potential

1. German Language Summary

Maligne Tumoren stellen heutzutage, gemeinsam mit kardiovaskulären Erkrankungen, die bedeutsamste Todesursache in Industrienationen dar[1,2]. Epidemiologische Studien prognostizieren darüber hinaus einen Anstieg der diesbezüglichen Krankheitslast um bis zu 50% innerhalb der nächsten 20 Jahre[3]. Während Neoplasien in allen Stadien eine erhebliche Morbidität und Reduktion der Lebensqualität verursachen, sind etwa 90% der Tumor-bedingten Todesfälle auf metastasierte Erkrankungsstadien zurückzuführen[4,5]. Da der hoch komplexe Prozess der Metastasierung zugleich den am wenigsten verstandenen Aspekt der Krebsbiologie darstellt[6], müssen Prävention, Diagnostik und Therapie von Stadium IV Tumoren auf Grundlage eines besseren molekularen und zellulären Verständnisses stetig weiterentwickelt werden.

Zu den Phasen der Disseminierung von Krebszellen zählen die Loslösung vom Primärtumor, die lokale Invasion des Tumor-umgebenden Stromas, das Eindringen in Blut- und Lymphgefäße, sowie die Extravasation in entfernten Geweben[7]. Eine Vielzahl von zellulären Subsystemen muss außerdem koordiniert zusammenspielen, um diese Prozesse zu ermöglichen. Dabei spielen diejenigen Signalwege eine zentrale Rolle, die zu einer erhöhten Zellmotilität führen, denn beinahe alle Stadien der Metastasierung setzen eine gerichtete Bewegung voraus[4,8]. Im Hinblick auf die physiologische Migration von Zellen ist seit langem bekannt, dass Calcium eines der wichtigsten Sekundärsignale darstellt, die Zellen zur Wanderung bewegen[9–11]. Zuletzt ist Calcium jedoch in zunehmendem Maße auch in der Krebsbiologie als Treiber von Motilität erkannt worden und eine Fülle von Kanälen, Pumpen und Calcium-bindenden Proteinen besitzt die Fähigkeit, physiologischerweise eng kontrollierte, intrazelluläre Calciumspiegel in Tumoren zu dysregulieren[12]. Das Calcium-bindende Protein Neuronal Calcium Sensor 1 (NCS-1) ist diesbezüglich von besonderem Interesse, da es eine wichtige physiologische Funktion für die Calciumhomöostase besitzt[13], Calciumsignale in verschiedensten Krankheiten dysreguliert[14] und eine erste Untersuchung einen präliminären Zusammenhang von NCS-1 mit Tumormetastasierung und reduziertem Patientenüberleben herstellen konnte[15].

In der vorliegenden Studie wurde deshalb einerseits der Einfluss von NCS-1 auf das Metastasierungsverhalten von Tumorzellen untersucht[16], auf der anderen Seite fand eine Korrelation von NCS-1 Leveln mit klinischen Parameter, insbesondere der Mortalität von Patienten mit hepatozellulärem Karzinom (HCC), statt[17]. Auf diese Weise konnte gezeigt werden, dass eine hohe NCS-1 RNA Expression in einer öffentlich verfügbaren HCC Kohorte mit einer ungünstigen Prognose assoziiert ist, wobei dies interessanterweise jedoch

ausschließlich auf Patienten asiatischer Abstammung zutraf. Dieses Ergebnis wurde in einer weiteren Kohorte validiert und um eine bioinformatische Analyse ergänzt, die LIM-Domain Kinase 1 (LIMK-1) als Protein identifizierte, das potentiell den Mittelpunkt eines NCS-1-abhängigen Signalnetzwerks darstellt. Da LIMK-1 Inhibitoren gegenwärtig in klinischer Erprobung sind[18], ist diese Signalachse ein vielversprechender pharmakologischer Angriffspunkt.

Um die Motilitätseffekte von NCS-1 zu untersuchen, wurde ein Zellmodell hergestellt, das NCS-1 stabil überexprimierte. Es zeigte sich im Vergleich zu der unveränderten Kontrollzelllinie nicht nur eine signifikante Änderung der Morphologie hin zu einem amöboiden Phänotypen. Auch die Migration in 2- und 3-dimensionalen Experimenten wurde durch NCS-1 deutlich verstärkt. Um den Prozess der Metastasierung zuletzt auch *in vivo* nachvollziehen zu können, wurden diese Zellen in die Schwanzvenen von gesunden Mäusen injiziert und deren Lungen bezüglich der Ausbildung von Filiae monitoriert. Unter dem Einfluss hoher NCS-1 Expression kam es zu einer deutlich verstärkten Absiedelung von Krebszellen mit größeren und vitaleren Tumoren nach 4 Wochen Wachstum. Mit diesen Experimenten ist erstmals gezeigt, dass NCS-1 nicht nur vielversprechendes Potential als klinischer Biomarker besitzt, sondern auch funktionell zur Metastasierung beiträgt. Zukünftigte Studien müssen erweisen, ob dysregulierte Calciumsignale oder die physische Interaktion von NCS-1 mit seinen Bindungspartner mechanistisch verantwortlich sind.

2. Introduction

Cancer is among the leading causes of disability and death world-wide[19,20]. Driven by changes in demographic structure and facilitated by risk factors like smoking and obesity[21], chronic cardiovascular disease and cancer are now responsible for up to 50% of all deaths in the Western world[1,22]. According to data from the German cancer registry[2], about 500,000 new cases were diagnosed in 2016 alone. In the same year, almost 230,000 fatalities were directly attributed to a malignant tumor. It is estimated that the burden of cancer will continue to rise globally, with a projected increase in prevalence of 47% between 2020 and 2040[3].

The role of prevention and early detection for counteracting these developments cannot be overstated[22,23]. However, many neoplasms are difficult to detect clinically or utilizing any one of the established screening tests[24]. A definitive diagnosis can oftentimes be made at an advanced stage only. This is especially true for certain malignancies of the GI tract[25,26] and ovarian cancer[24]. Even in cases of early diagnosis and after complete surgical resection of the primary tumor, the presence of nodal micro-metastasis is associated with a considerable risk of relapse compared to node-negative cases[27]. Because detection of nodal metastases < 2 mm in size is a major challenge for pathologists[28], effective treatment options for these patients are urgently needed. Nevertheless, and despite considerable advances in the treatment of metastatic tumors through the introduction of tyrosine kinase inhibitors[29] and, more recently, immunotherapy[30], survival of patients with stage IV disease remains poor[6].

Considering all of this, the furthering of our understanding of metastasis formation and dissemination of tumor cells throughout the body is of paramount importance. To that end, this study examines the Calcium- (Ca^{2+}) binding protein Neuronal Calcium Sensor 1 (NCS-1) as a dysregulator of cellular Ca^{2+} signaling, contributor to metastatic spread and predictor of an adverse disease outcome in certain patients.

2.1 Tissue Invasion and Metastatic Dissemination are Hallmarks of Cancer

As described above, local tissue invasion and the spread of tumor cells to distant sites is among the clinically most relevant of the eight “Hallmarks of Cancer” as proposed by Weinberg and Hanahan[8]. Nevertheless, the complex processes involved are often considered the least understood area of cancer research[5]. Cancerous colonization of remote tissue constitutes the final step of an entire sequence of events, each requiring the interplay of multiple, aberrant molecular pathways to overcome the body’s defensive measures[7,31]. Importantly, cell motility has been identified as a key prerequisite for most of the steps involved, notably the invasion of the tumor-surrounding stroma, intravasation (i.e. the ability

of cells to enter blood and lymphatic vessels), migration through the bloodstream and extravasation (i.e. the capability of cells to exit the vascular system)[7,11,31]. In the following section, a range of pathways that confer a motility advantage to cancer cells will be reviewed.

2.1.1. A Wide Range of Molecular Pathways Contributes to Metastasis Formation via Increased Cell Motility

Studies using cultured cancer cells, organoids, and simple model organisms like Drosophila melanogaster and zebrafish[11] have elucidated the contribution of various molecular mechanisms to malignant cell migration, invasion, and ultimately metastatic spread. One of the earliest incidents in the chain of events is the redistribution of cytoskeletal proteins, which polarizes cells and prepares them for migration. This morphological transformation can be induced by chemokine signaling via G-protein coupled receptors (GPCRs) and cAMP[32], by increases in intracellular Ca^{2+} and IP_3[33] or by dysregulation of the PIP_3-PI3K-PKB cascade[34]. All three pathways are frequently altered in neoplastic cells[11] and inhibitors of the PI3K-AKT signaling axis are actively investigated with regards to their anti-tumor activity[35].

Whereas different modes of single- and multi-cell migration have been identified, amoeboid motility is proposed to be a feature of especially malignant tumor cells with high metastatic potential[36,37]. A key regulator of the amoeboid migratory phenotype is the RHO-associated protein kinase (ROCK)[18,36,38] and its downstream target LIM-domain kinase 1 (LIMK-1)[39,40]. ROCK orchestrates a plethora of cellular processes including the phosphorylation and thus remodeling of the actin cytoskeleton, the formation of focal and cellular adhesions, and the buildup of stress fibers[38,39,41,42], all of which are prerequisites for directional cell movement. Consequently, inhibiting this signaling network whenever it is highly expressed or its components are mutated, is proposed as a promising therapeutic opportunity[38].

To be able to penetrate the basement membrane and invade into the underlying stroma, transformed epithelial cells were observed to form so-called invadopodia[43]. These actin-rich protrusions then secret matrix metalloproteinases (MMPs)[44], which are Ca^{2+}-dependent enzymes capable of degrading laminin and other components of the basement membrane. Like in amoeboid cell movement, RHO GTPases like RhoA[38,45] and Rac1[46] are core components of the underlying machinery that leads to the necessary restructuring of the actin cytoskeleton. The latter together with RHO GTPase activity and focal adhesion protein turnover is tightly regulated by intracellular Ca^{2+} signaling[47–49].

Whereas differentiated epithelial cells are programmed to undergo apoptosis when not attached to a basement membrane[50], epithelial-to-mesenchymal transition (EMT) is

controversially discussed[51] as a mechanism by which neoplastic cells can survive long after detachment[4]. In addition, a mesenchymal phenotype is accompanied by increased motility and possibly chemotherapy resistance[36]. On a molecular level, EMT can be induced by various extracellular as well as intracellular signals and is characterized by high expression levels of the key transcription factors SNAIL1, TWIST, ZEB1 and ZEB2[4]. On the other hand, the adhesion protein cadherin 1 (CDH-1), which is pivotal to the coherence of epithelia, is expressionally suppressed[52]. The plasticity and aggressiveness that EMT confers to tumor cells makes it an attractive target for therapeutic interventions and promising approaches are currently being investigated[53]. Finally, there is considerable overlap between EMT and Ca^{2+} signaling. Peaks in cytoplasmic Ca^{2+} can actively induce EMT[54] and simultaneously promote motility and invasiveness. Because it is such a vital component of most of the pathways described, the next section discusses Ca^{2+} as a driver of physiological and metastatic cell movement.

2.1.2. Calcium is an Important Downstream Effector of Motility Pathways And Frequently Dysregulated in Aggressive Tumors

Ca^{2+} gradients play a role in almost all cellular processes, including programmed cell death, transcriptional regulation, cell-to-cell signaling, membrane electrophysiology, and motility[10]. Mammalian cells possess a sophisticated apparatus of Ca^{2+} binding proteins, pumps and channels that work together to keep the intracellular Ca^{2+} concentration at levels as low as ~100nM[9]. The canonical mechanism leading to transient bursts in free Ca^{2+} is the ligand-dependent activation of GPCRs, followed by the production of IP_3, which activates IP_3-receptors (IP_3R). IP_3Rs are Ca^{2+} channels that are localized in the membrane of the endoplasmic reticulum (ER) and they activate the Ca^{2+}-sensitive ryanodine receptors (RYR), another ER Ca^{2+} channel that further amplifies the spike in concentration[55–57]. In addition to this highly conserved cascade, a diverse set of signaling pathways can give rise to fluctuations in Ca^{2+}. Figure 1 provides an outline of the components involved, including many of the molecules discussed in the previous section as well as downstream effectors described in the following paragraph.

Free Ca^{2+} above the resting level binds troponins in skeletal and cardiac muscle[10], elicits smooth muscle contraction by the activation of myosin light-chain kinase (MLCK), and modulates shape and movement of various cell types through motor proteins like myosin, dynein and kinesin[58]. Additionally, Ca^{2+}-binding proteins like calmodulin (CALM) and S100 proteins mediate a large subset of the cellular effects of Ca^{2+} upon binding. Downstream pathways are responsible for the regulation of gene expression via calcineurin and the Ca^{2+}-

dependent transcription factor NFAT, for cell growth, differentiation and proteolysis, and for the dynamics of the cytoskeleton[59].

Motivated by these crucial physiological functions of Ca^{2+} signals, their dysregulation has naturally been investigated in the context of malignancy. Indeed, it has been found that up- or down-regulation of almost all parts of the cascade can contribute to carcinogenesis and metastasis via the perturbation of Ca^{2+} homeostasis[12]. Examples of dysregulators of the latter are transient receptor potential (TRP) and store-operated Ca^{2+} (SOC) channels[60–62], the IP_3R[63], the S100 family of Ca^{2+}-binding proteins[64,65], calmodulin[66,67], GPCRs[68], and, as focus of attention of this study, NCS-1[15–17].

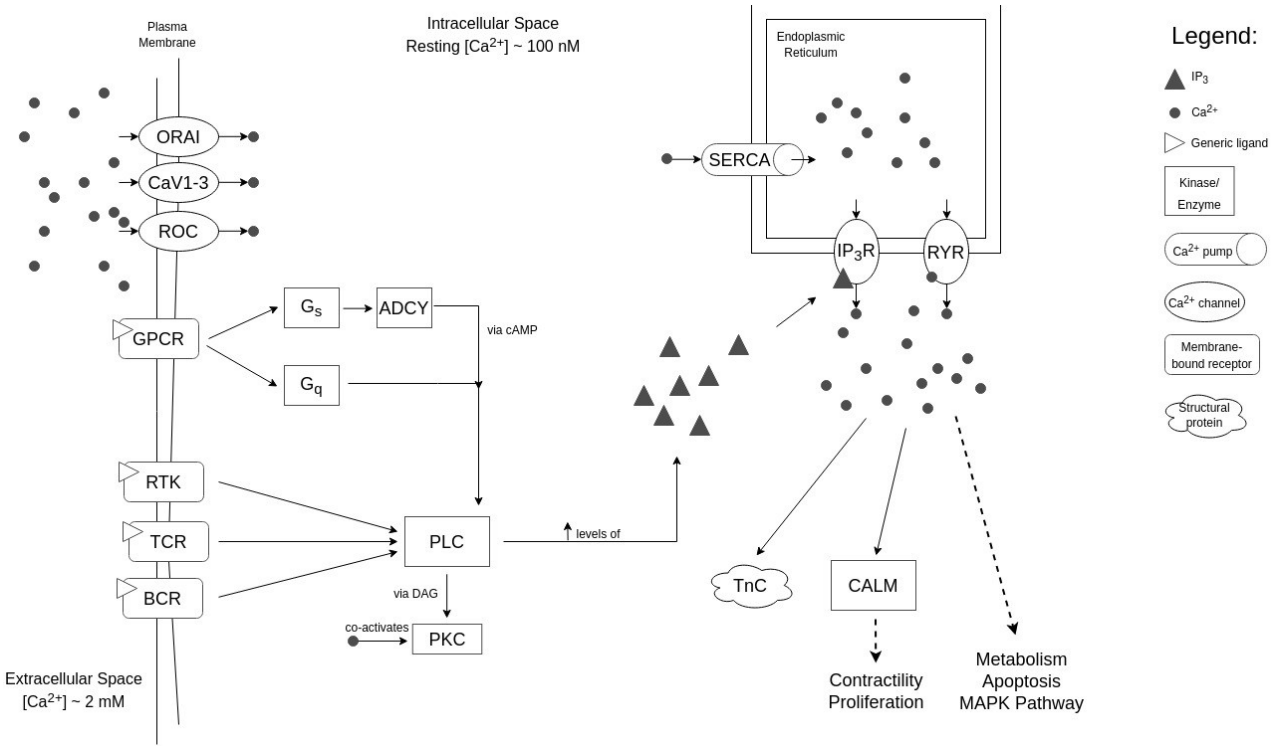

Figure 1: Intracellular Ca^{2+} signaling pathway. The schematic is derived from the Kyoto Encyclopedia of Genes and Genomes[111] as well as the references mentioned throughout the introduction. Only those components are shown that are most relevant to this study. The mitochondria represent an additional important intracellular Ca^{2+} store but are omitted to improve readability.

2.2 Neuronal Calcium Sensor 1 Regulates Calcium Signaling in Health and Disease

As delineated in the preceding sections, Ca^{2+} is of great physiological importance, with far reaching implications for cancer biology. In the ensuing sections, NCS-1 is introduced as a

player on both sides of the Ca^{2+} signaling spectrum. Particular emphasis is placed on well-established disease associations.

2.2.1. Molecular and Cellular Characteristics of Neuronal Calcium Sensor 1

NCS-1 is a small (22kDa), highly conserved, almost ubiquitously expressed, cytosolic Ca^{2+}-binding protein[14]. Subsequent to the initial discovery of frequinin, the equivalent of human NCS-1 in Drosophila[69], homologs were identified in a diversity of organisms ranging from mammals to yeast[70]. The resolved crystal structure of NCS-1 (see figure 2) revealed features similar to other members of the NCS protein family like recoverin and neurocalcin[71], most notably four helix-loop-helix motifs, so-called EF-hand domains, and an N-terminal myristoyl group[72]. Three of the four EF-hands are capable of binding Ca^{2+} at low concentrations, whereas the fourth pseudo-EF-hand domain functions as a stabilizer of overall protein conformation. The effects of protein myristoylation are diverse and actively investigated[73], most likely allowing for Ca^{2+}-dependent association of NCS-1 to membranes as well as co-localization with downstream signaling targets[74].

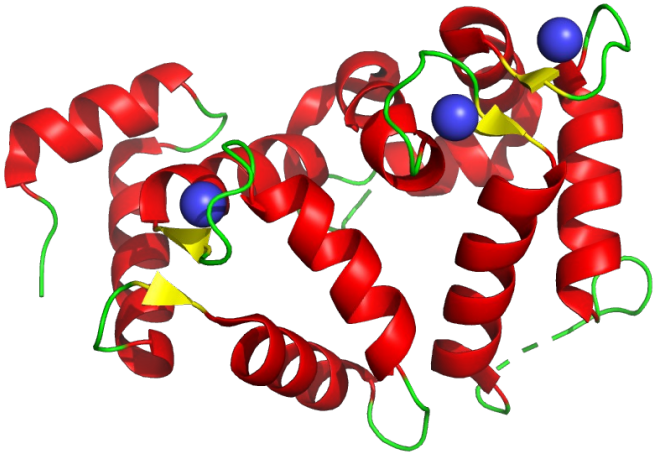

Figure 2: Molecular structure of NCS-1 (PDB identifier 4GUK, illustration created using PyMOL v2.5.0). Helices are colored in red, sheets in yellow, and loops in green. Blue Ca^{2+} ions are complexed by the three functional EF hand domains which consist of a short loop between two alpha helices. In addition, a fourth, stabilizing pseudo-EF-hand motif is located below the leftmost Ca^{2+} atom.

In vitro investigation of purified NCS-1 demonstrated its high affinity but low capacity for Ca^{2+} binding[75], hinting towards a role as a signaling molecule rather than a buffer of free Ca^{2+}. And indeed, NCS-1 is implicated in various pathways. For historical reasons, NCS-1 function has been explored most extensively in neural cells and models of the brain. Studies found that

neuronal plasticity, i.e. axon and dendrite development as well as regeneration from injury[76–78], critically depends on NCS-1, as does the secretion of neurogranules via exocytosis[79,80], intracellular vesicle trafficking between Golgi network and plasma membrane[81,82], and therefore overall synaptic function[13]. In NCS-1 knockout mice, motivation, learning, and memory are consistently and significantly diminished and overall neurodevelopment is impaired[83,84]. In terms of a molecular mechanism, collective evidence suggests that NCS-1 elicits its effects in part through the physical modulation of the Dopamine D2 receptor, a transcriptional network of differentially expressed genes, and the overall disruption of Ca^{2+} homeostasis[85–88].

Furthermore, NCS-1 physically interacts with the IP_3R[89], a key component of Ca^{2+} signaling that was reviewed above. Upon binding of IP_3-activated channels, the influx of Ca^{2+} increases in a dose-dependent manner[90]. Studies in cardiac myocytes confirmed this modulatory effect in tissues outside of the nervous system[91]. Beyond that, NCS-1 modulates the activity of downstream targets of Ca^{2+} like calmodulin[92] and the PI3K/PKB pathway[93].

Many more interactions of NCS-1 with cellular proteins like Interleukin-1 receptor accessory protein-like 1 (IL1RAPL), Adenosine A2 receptor (ADORA2A), and G-Protein coupled receptor kinase 2 (GRK2) are described in a growing body of literature[14], but their specific biological functions need to be clarified in future research endeavors.

2.2.2. NCS-1 is Implicated in Multiple Neurological and Psychiatric Diseases

Originating from its vital role for development and plasticity of the nervous system, NCS-1 was investigated in the context of several neurological and psychiatric diseases. It has been found that alterations of NCS-1 contributes to a wide spectrum of conditions, from addiction[94], autism[95,96], and Parkinson's disease[97] to bipolar disorder and schizophrenia[98,99]. Chemotherapy-induced peripheral neuropathy (CIPN), a condition in which peripheral nerves are damaged by cancer therapeutics like paclitaxel, can be aggravated by the interaction of NCS-1 with the responsible cytotoxic agent[90,100]. Clarification of the underlying mechanisms[14] has facilitated the development of a promising therapeutic approach that re-purposes the psychiatric drug lithium and that is currently in early pre-clinical and clinical testing[101]. In light of these insights, the role of NCS-1 in chemotherapy-induced cognitive decline is actively being researched as well[102].

2.2.3. High Levels of NCS-1 are Associated with Poor Breast Cancer Outcome

Previous to the present study, first evidence linking NCS-1 to the promotion of metastasis and tumor aggressiveness was presented by Moore and colleagues[15]. The authors firstly

examined the effects of stable NCS-1 overexpression on the MCF-7 and MB-231 breast cancer cell lines. Compared to the wild-type, NCS-1^{high} cells showed a marked increase in migratory activity and reduced cell-matrix adhesion. This phenotype could be reversed by knocking down the overexpressed NCS-1 using an shRNA approach. Secondly, two independent cohorts comprising 515 and 301 breast cancer patients respectively, were histologically assessed. Immunohistochemical staining for NCS-1 revealed significantly higher protein levels in tissue from patients with poor disease outcome and unfavorable clinical characteristics like lymph node positivity and larger tumor size.

Collectively, the presented data provides strong evidence that NCS-1 renders breast cancer cells more motile and might serve as a prognostic biomarker. Further studies are warranted to validate these findings in other tumor entities and establish a molecular mechanism by which NCS-1 elicits its effects. The present study makes an attempt at both.

2.3 Research Questions

To conclude, the fast-paced increase in the global burden of cancer as well as insights from tumor biology underscore the pressing need to more deeply understand the process of metastasis formation. Whereas many biological mechanisms facilitate cancer cell spread, increased motility has been proven to contribute to multiple of its phases. Based on the established importance of Ca^{2+} for cell movement, on the role of NCS-1 as a Ca^{2+} dysregulator, and on previous laboratory and clinical observations[15], this study aims to:

1. Measure NCS-1 RNA in tumor samples versus normal tissue to confirm an increase of expression beyond physiological levels during carcinogenesis,

2. Retrospectively investigate the capacity of NCS-1 expression levels to predict cancer patient outcome in a tumor type other than breast cancer,

3. Leverage an unbiased bioinformatics analysis to put NCS-1 into the context of a broader signaling network, potentially discovering novel therapeutic targets,

4. Assess the effects of NCS-1 overexpression on cellular and mouse models of cancer to consolidate the link between dysregulated Ca^{2+} signaling and increased tumor cell spread.

3. Materials and Methods

Materials and methods that were used to produce the results discussed below are published elsewhere[16,17].

4. Results

The results discussed below are published elsewhere[16,17].

5. Discussion

As outlined in the introduction, a metastatic phenotype is not only a hallmark of cancer cells but also of utmost clinical importance, considering the fact that approximately 90% of tumor related deaths[7] occur in the context of stage IV (i.e. metastatic) disease. It was highlighted that cellular motility, a process that is oftentimes driven by Ca^{2+} signals[60], contributes to most of the biological steps leading to tumor cell dissemination[11]. Thus, the research question was posed whether the Ca^{2+}-binding protein NCS-1 with its diverse biological and disease implications might favor the spread of tumor cells throughout the body. More precisely, it was asked whether high NCS-1 expression levels are firstly associated with poor patient outcome and secondly lead to an invasive phenotype *in vitro* and *in vivo*. To investigate these issues, two studies were conducted which are discussed in the following sections.

5.1 High NCS-1 Expression Levels are Associated with Poor Patient Outcome

Because a link between patient outcome and NCS-1 protein levels was already established for breast cancer[15], the first study[17] focused on hepatocellular carcinoma (HCC) as another tumor entity with similarly high demand for clinical biomarkers and novel therapeutic strategies[103].

5.1.1. NCS-1 Expression Levels are Upregulated During Carcinogenesis

Data from publicly accessible sources was used to test the hypothesis that NCS-1 expression levels are comparatively low in physiologically differentiated hepatocytes and subsequently up-regulated during carcinogenesis. And indeed, analyzing RNA sequencing data of 348 HCC cases from The Cancer Genome Atlas (TCGA)[104] and comparing NCS-1 expression levels to measurements done in healthy liver tissue (likewise retrieved from external databases) revealed significantly higher NCS-1 in the malignancies. Interestingly, the distribution of data points was much wider for samples from the TCGA, suggesting considerable heterogeneity between individual cases in the cohort.

To validate this finding, a commercially available micro array comprising 47 histological HCC specimens as well as 41 matched, adjacent non-neoplastic tissue cores was examined using immunohistochemistry (IHC). Again, NCS-1 protein levels were significantly higher in neoplastic samples, reinforcing the presented hypothesis. Furthermore, IHC scores of carcinomas did not correlate with protein levels of their matched stromal samples, making

high baseline expression in healthy hepatocytes an unlike prerequisite for NCS-1 increases during tumor development.

5.1.2. Survival of Asian HCC Patients is Retrospectively Associated with NCS-1 Levels

To assess the ability of NCS-1 to predict disease outcome in HCC, clinical data provided by the TCGA was included into the analysis. Whereas expression levels were not generally higher in patients surviving beyond the follow-up period, stratification according to race yielded the following results: Asian patients who succumbed to their tumor were more likely to have exceptionally high NCS-1 levels than Asians surviving the disease. Due to the relatively small size of this subgroup, significant p-values were only observed for Asian males. To better understand possible differences in NCS-1 expression between Asian and white patients, the latter being the only subgroup in the dataset with a sample size sufficiently large for proper analysis, a binary classification of samples into an NCS-1^{high} and NCS-1^{low} group was established. A receiver operating characteristic curve was utilized to establish an appropriate cutoff for continuously distributed expression values. While patients that were subsequently categorized as NCS-1^{low} presented with the consistently low expression levels as expected (levels that were independent of race and also virtually free of variability), NCS-1^{high} Asians presented with much higher average NCS-1 compared to their white counterparts ($p = 0.056$). Additionally, contingency tables partitioning patients according to NCS-$1^{high/low}$ and survival status revealed significantly higher odds of death in the presence of high NCS-1 in the Asian sub-population. The same analysis performed for white patients proved to be non-significant.

Finally, time series analyses were performed using Kaplan-Meier plots. To achieve greater external validity, an additional cohort of 231 Asian HCC patients was retrieved from the ICGC database[105]. The subgroup of NCS-1^{high} patients exhibited significantly worse survival over time, an observation that was made for Asians from the TCGA cohort as well as all patients from the ICGC cohort. Here again, NCS-1 status did not correlate with outcome when only white patients were considered.

One explanation for the observed race-dependent, non-uniform role of NCS-1 in HCC carcinogenesis is provided by the fact that multiple risk factors like exposure to toxins (especially to ethyl alcohol and aflatoxin), chronic virus hepatitis, metabolic factors like diabetes and fatty liver disease, and many more contribute to carcinoma development. It is well known throughout the literature that the distribution of these risk factors varies

significantly with race and geographic location[106] and that these differences are reflected in distinct genomic profiles of the eventual HCC[107,108].

In conclusion, this study identifies an especially lethal subgroup of hepatocellular carcinomas that is characterized by high NCS-1 expression levels. Due to its retrospective nature, it suggests NCS-1 as a predictive biomarker that needs to be validated in prospective trials. Furthermore, additional studies are called for to better understand how NCS-1 up-regulation is linked to clinical attributes like subgroup-specific risk factors and genomic features. This way, NCS-1 might not only prove useful as a biomarker but also for targeted prevention.

5.1.3. A Co-Expression Network Demonstrates the Relationship of NCS-1 with Motility Pathways

Even though high expression of NCS-1 is associated with poor patient survival, the molecular mechanisms through which it operates remain to be elucidated. To provide a starting point for future studies, linear regression techniques were employed to systematically correlate NCS-1 with 60 483 transcripts across all 348 cases in the TCGA HCC dataset. This unbiased bioinformatics approach showed that LIMK-1 was most strongly co-expressed with NCS-1 by a large margin (Pearson's $r = 0.76$, $p < 0.0001$), a finding that could be reproduced in the ICGC cohort of Asian HCC patients (Pearson's $r = 0.72$, $p < 0.0001$). To maximize robustness of the analysis, 3 additional cohorts of breast cancer, lung adenocarcinoma and lung squamous cell carcinoma patients were retrieved from the TCGA and co-expression networks were constructed. Across these different entites, NCS-1 was consistently co-expressed with proteins from cellular motility pathways like (actin) cytoskeleton regulation, focal adhesion and cell junction organization, RHO GTPase signaling (including LIMK-1 as a downstream target), and microtubule-based processes. Figure 3 summarizes the crucial parts of the newly discovered signaling axis.

Lastly, Broad Institute's Cancer Cell Line Encyclopedia (CCLE) database was queried for expression data of 1019 cancer cell lines. Not only did LIMK-1 correlate positively with NCS-1 in breast and liver cancer-derived CCLE cell lines, thus validating the previous findings. There was also no observable correlation of the two genes in lymphoma and leukemia cell lines.

5.1.4. Conclusion

Taken together, the conducted in silico experiments suggest that NCS-1 elicits its effects via an entire network of motility pathways, most importantly the ROCK/LIMK-1 signaling cascade

and actin polymerization dynamics (see figure 3 for an overview). Interestingly, lymphoma and leukemia cells which originate from highly motile precursor cells that have an inherent capacity to travel through the blood stream, do not seem to exploit this newly identified signaling axis.

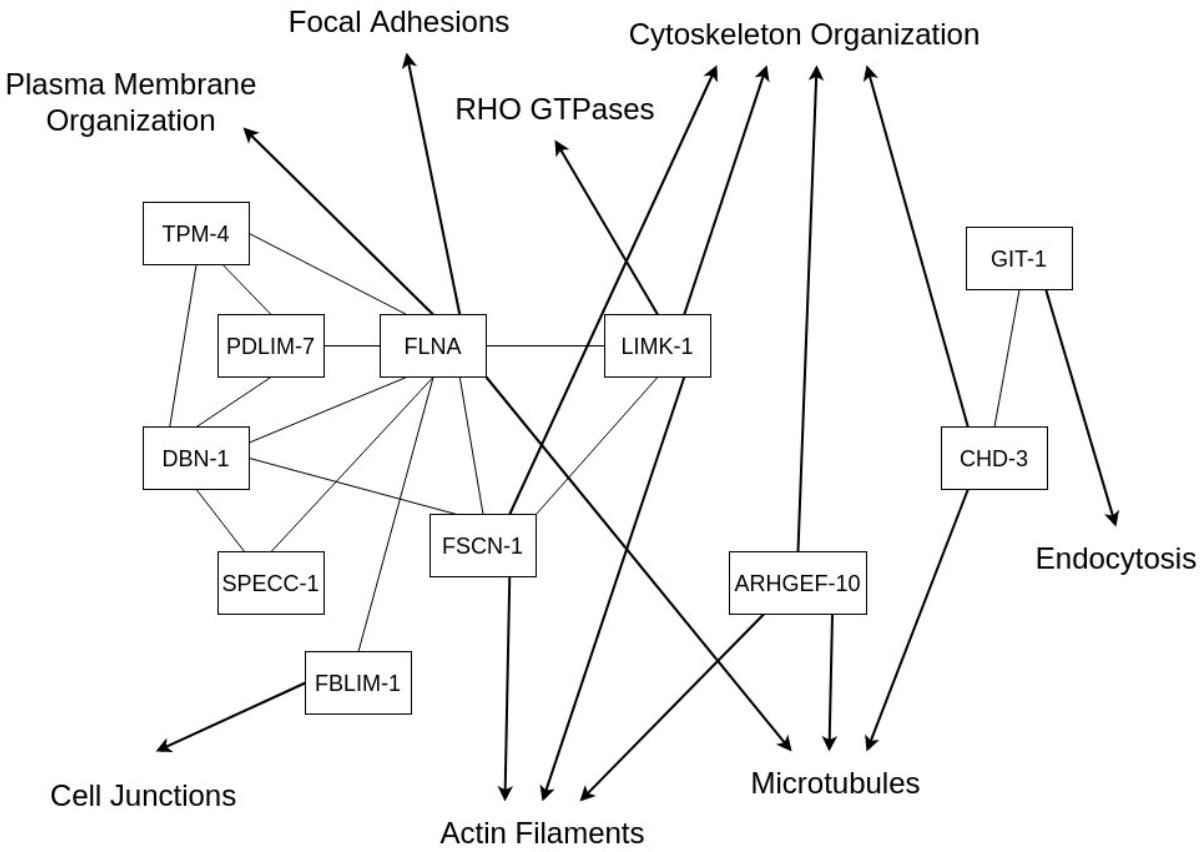

Figure 3: NCS-1 co-expression network derived from the more extensive network in Schuette et al.[17]*. All genes displayed are consistently co-expressed with NCS-1 across different tumor entities. The software tool EGAN*[112] *was used to compile pathway information from various databases and RNA sequencing data into this association network.*

Again, a major limitation of the above approach is its retrospective, correlative nature. It remains to be shown that NCS-1 is causally linked to the genes that were found to be co-expressed. As pointed out in the introduction, NCS-1 might physically interact with some of them while affecting the expression or activity of others via dysregulated Ca^{2+} signals. Because LIMK-1[109] and ROCK inhibitors[18] are readily available and considering the scarcity of effective therapies for advanced HCC[103], future studies are needed to evaluate the activity of these inhibitors in NCS-1^{high} models of HCC.

5.2 Overexpression of NCS-1 Induces a Motile, Metastatic Phenotype in Cellular and Mouse Experiments

After retrospectively investigating its utility as a biomarker, a second study[16] was conducted to causally link NCS-1 overexpression to increased invasiveness, motility and metastasis formation. As discussed below, a 3-dimensional cellular model was employed alongside a mouse xenograft to expand on the experiments by Moore and colleagues, which were conducted using a 2-dimensional *in vitro* design only[15].

5.2.1. NCS-1 Induces Morphological Changes and a Motility Phenotype Without Increasing Proliferation

Because acquisition of an amoeboid phenotype is one route via which cancer cells become more motile and aggressive, the morphology of NCS-1 overexpressing cells was systematically assessed. To this end, the triple-negative MDA-MB-231 breast cancer cell line was virally transduced with an NCS-1 plasmid and stable overexpression (OE) was confirmed by immunoblotting as well as quantitative RT-PCR analysis. Subsequent brightfield microscopy revealed a significant increase in cell size (as measured by aspect ratio) and reduced circularity of these NCS-1^{OE} cells compared to the wildtype (NCS-1^{wt}). On the other hand, a proliferation assay monitoring cellular ATP content over a period of 5 days did not show differences in growths rates between NCS-1^{OE} and NCS-1^{wt} cell lines. This finding suggests that NCS-1 overexpression is sufficient to transform cellular morphology without negatively impacting survival signaling, thus conferring an overall evolutionary advantage to cancer cells. The previously established hypothesis that NCS-1 elicits its effects via interaction with LIMK-1 and the actin cytoskeleton was further substantiated by confocal microscopy. In both lines of MDA-MB-231 cells, NCS-1 localized primarily to cellular protrusions and to actin filaments at the leading edge but not to stress fibers or cytoplasmic actin puncta. Because tightly controlled spatiotemporal Ca^{2+} signals at the leading edge are of paramount importance for cell movement, colocalization of NCS-1 with these components might hint at a functional relationship.

As a next logical step, the cell model was cultivated in 2 dimensions. In line with previously published results[15], MDA-MB-231 cells expressing high levels of NCS-1 covered petri dishes faster in a colony formation experiment and closed wounds more quickly in a scratch assay. To be able to recreate the 3-dimensional context of *in vivo* tumor metastasis more realistically, NCS-1^{OE} and NCS-1^{wt} cells were then cultivated in collagen gels and time-lapse confocal microscopy was used to measure average movement speed and distance over a period of 8 hours. And indeed, NCS-1^{OE} cells moved significantly farther distances and did so more quickly. It can be concluded that high levels of NCS-1 are sufficient to make cancer

cells more motile in 2 and 3 dimensions, without degrading cellular health in ways that reduce proliferation.

5.2.2. Cancer Cells Harboring High Levels of NCS-1 are More Capable of Forming Distant Metastases in a Mouse Xenograft Model

In an attempt to model *in vivo* metastasis even more closely, a mouse xenograft model was established. MDA-MB-231 NCS-1^{OE} and NCS-1^{wt} cells that also carried a luciferase reporter gene were injected into the tail veins of otherwise healthy mice and photon flux was measured over the lungs at specific time points as a surrogate for tumor size. Finally, lung tissue was harvested after euthanization of all animals on day 28 of the experiment. As would be expected from the *in vitro* studies, lung metastases formed more rapidly from NCS-1^{OE} cells. The most profound difference in lung tumor size could be observed between days 1 and 7. After 7 days however, established lung tumors grew at identical rates. Thus, here too, a significant effect of NCS-1 on motility and invasiveness could be observed. High expression levels positively impacted the ability of MDA-MB-231 cells to extravasate and locally invade into healthy lung tissue. On the other hand, whereas fewer NCS-1^{wt} cells succeeded in these early phases of metastasis, proliferation rates of established tumors were virtually identical, irrespective of NCS-1 status.

Finally, histopathological examination of build-up lung tumors after 28 days of growth provided additional support for this interpretation. Malignancies stemming from NCS-1^{wt} cells displayed large areas of necrosis in almost all mice, with practically no signs of cell death in NCS-1^{OE} metastases. Considering the imaging data, NCS-1 therefore seems to facilitate survival during early engraftment by a yet unknown mechanism. Future studies need to investigate the processes by which NCS-1 aids tumor cells in surviving the first expansion phase.

5.2.3. Conclusion

In conclusion, the pro-metastatic role of NCS-1 seems to be consistent across all *in vitro* and *in vivo* models of neoplastic dissemination that were examined. With this study, important starting points for an investigation into the underlying molecular mechanisms are established. However, further research is certainly required, not least because the present study was limited to one highly aggressive, triple-negative breast cancer cell line. Considering the Ca^{2+} dependent regulation of LIMK-1[110], its important role for actin cytoskeleton organization, and the consistent co-expression with NCS-1[17], LIMK-1 inhibition constitutes a promising therapeutic approach that needs to be studied in depth. Last but not least, up to the present

the genomic alterations that cause NCS-1 overexpression were not looked into. Structural knowlegde about the NCS-1 locus might improve its usefulness as a biomarker in times, where genomic data is becoming increasingly accessible in routine clinical practice.

6. Bibliography

1 Heron M. Deaths: Leading Causes for 2017. *Natl Vital Stat Reports* 2019; **68**. DOI:10.15620/cdc:104186.

2 Cancer in Germany 2015/2016, 12th edn. Berlin: Robert Koch Institute (ed.) and the Association of Population-based Cancer Registries in Germany (ed.), 2020.

3 Sung H, Ferlay J, Siegel RL, *et al.* Global Cancer Statistics 2020: GLOBOCAN Estimates of Incidence and Mortality Worldwide for 36 Cancers in 185 Countries. *CA Cancer J Clin* 2021; **71**: 209–49.

4 Brabletz T, Kalluri R, Nieto MA, Weinberg RA. EMT in cancer. *Nat Rev Cancer* 2018; **18**: 128–34.

5 Lambert AW, Pattabiraman DR, Weinberg RA. Emerging Biological Principles of Metastasis. *Cell* 2017; **168**: 670–91.

6 Chaffer CL, Weinberg RA. A Perspective on Cancer Cell Metastasis. *Science* 2011; **331**: 1559–64.

7 Seyfried TN, Huysentruyt LC. On the Origin of Cancer Metastasis. *Crit Rev Oncog* 2013; **18**: 43–73.

8 Hanahan D, Weinberg RA. Hallmarks of Cancer: The Next Generation. *Cell* 2011; **144**: 646–74.

9 Berridge MJ. Calcium signalling and cell proliferation. *Bioessays* 1995; **17**: 491–500.

10 Clapham DE. Calcium Signaling. *Cell* 2007; **131**: 1047–58.

11 Stuelten CH, Parent CA, Montell DJ. Cell motility in cancer invasion and metastasis: insights from simple model organisms. *Nat Rev Cancer* 2018; **18**: 296–312.

12 Stewart TA, Yapa KTDS, Monteith GR. Altered calcium signaling in cancer cells. *Biochimica et Biophysica Acta (BBA) - Biomembranes* 2015; **1848**: 2502–11.

13 Dason JS, Romero-Pozuelo J, Atwood HL, Ferrús A. Multiple Roles for Frequenin/NCS-1 in Synaptic Function and Development. *Mol Neurobiol* 2012; **45**: 388–402.

14 Boeckel GR, Ehrlich BE. NCS-1 is a regulator of calcium signaling in health and disease. *Biochimica et Biophysica Acta (BBA) - Molecular Cell Research* 2018; **1865**: 1660–7.

15 Moore LM, England A, Ehrlich BE, Rimm DL. Calcium Sensor, NCS-1, Promotes Tumor Aggressiveness and Predicts Patient Survival. *Mol Cancer Res* 2017; **15**: 942–52.

16 Apasu JE, Schuette D, Laranger R, *et al.* Neuronal calcium sensor 1 (NCS1) promotes motility and metastatic spread of breast cancer cells *in vitro* and *in vivo*. *FASEB j* 2019; **33**: 4802–13.

17 Schuette D, Moore LM, Robert ME, Taddei TH, Ehrlich BE. Hepatocellular Carcinoma Outcome Is Predicted by Expression of Neuronal Calcium Sensor 1. *Cancer Epidemiol Biomarkers Prev* 2018; **27**: 1091–100.

18 Lee M-H, Kundu JK, Chae J-I, Shim J-H. Targeting ROCK/LIMK/cofilin signaling pathway in cancer. *Arch Pharm Res* 2019; **42**: 481–91.

19 Ferlay J, Soerjomataram I, Dikshit R, *et al.* Cancer incidence and mortality worldwide: Sources, methods and major patterns in GLOBOCAN 2012. *Int J Cancer* 2015; **136**: E359–86.

20 Vos T, Lim SS, Abbafati C, *et al.* Global burden of 369 diseases and injuries in 204 countries and territories, 1990–2019: a systematic analysis for the Global Burden of Disease Study 2019. *The Lancet* 2020; **396**: 1204–22.

21 Vineis P, Wild CP. Global cancer patterns: causes and prevention. *The Lancet* 2014; **383**: 549–57.

22 Ryerson AB, Eheman CR, Altekruse SF, *et al.* Annual Report to the Nation on the Status of Cancer, 1975-2012, featuring the increasing incidence of liver cancer. *Cancer* 2016; **122**: 1312–37.

23 Valle I, Tramalloni D, Bragazzi NL. Cancer prevention: state of the art and future prospects. *J Prev Med Hyg* 2015; **56**: E21–7.

24 Hori SS, Gambhir SS. Mathematical Model Identifies Blood Biomarker–Based Early Cancer Detection Strategies and Limitations. *Sci Transl Med* 2011; **3**. DOI:10.1126/scitranslmed.3003110.

25 Van Cutsem E, Sagaert X, Topal B, Haustermans K, Prenen H. Gastric cancer. *The Lancet* 2016; **388**: 2654–64.

26 Kamisawa T, Wood LD, Itoi T, Takaori K. Pancreatic cancer. *The Lancet* 2016; **388**: 73–85.

27 Gwóźdź P, Pasieka-Lis M, Kołodziej K, *et al.* Prognosis of Patients With Stages I and II Non-Small Cell Lung Cancer With Nodal Micrometastases. *Ann Thorac Surg* 2018; **105**: 1551–7.

28 Chuang W-Y, Chen C-C, Yu W-H, *et al.* Identification of nodal micrometastasis in colorectal cancer using deep learning on annotation-free whole-slide images. *Mod Pathol* 2021; **34**: 1901–11.

29 Pottier C, Fresnais M, Gilon M, Jérusalem G, Longuespée R, Sounni NE. Tyrosine Kinase Inhibitors in Cancer: Breakthrough and Challenges of Targeted Therapy. *Cancers* 2020; **12**: 731.

30 Liu L, Bai X, Wang J, *et al.* Combination of TMB and CNA Stratifies Prognostic and Predictive Responses to Immunotherapy Across Metastatic Cancer. *Clin Cancer Res* 2019; **25**: 7413–23.

31 Pachmayr E, Treese C, Stein U. Underlying Mechanisms for Distant Metastasis - Molecular Biology. *Visc Med* 2017; **33**: 11–20.

32 Nichols JM, Veltman D, Kay RR. Chemotaxis of a model organism: progress with Dictyostelium. *Current Opinion in Cell Biology* 2015; **36**: 7–12.

33 Hříbková H, Grabiec M, Klemová D, Slaninová I, Sun Y-M. Calcium signaling mediates five types of cell morphological changes to form neural rosettes. *J Cell Sci* 2018; **131**: 1–12.

34 Xue G, Hemmings BA. PKB/Akt-Dependent Regulation of Cell Motility. *JNCI Journal of the National Cancer Institute* 2013; **105**: 393–404.

35 Alzahrani AS. PI3K/Akt/mTOR inhibitors in cancer: At the bench and bedside. *Seminars in Cancer Biology* 2019; **59**: 125–32.

36 Graziani V, Rodriguez-Hernandez I, Maiques O, Sanz-Moreno V. The amoeboid state as part of the epithelial-to-mesenchymal transition programme. *Trends in Cell Biology* 2022; **32**: 228–42.

37 Yamada KM, Sixt M. Mechanisms of 3D cell migration. *Nat Rev Mol Cell Biol* 2019; **20**: 738–52.

38 Clayton NS, Ridley AJ. Targeting Rho GTPase Signaling Networks in Cancer. *Front Cell Dev Biol* 2020; **8**: 222.

39 Scott RW, Hooper S, Crighton D, *et al.* LIM kinases are required for invasive path generation by tumor and tumor-associated stromal cells. *Journal of Cell Biology* 2010; **191**: 169–85.

40 Prunier C, Prudent R, Kapur R, Sadoul K, Lafanechère L. LIM kinases: cofilin and beyond. *Oncotarget* 2017; **8**: 41749–63.

41 Scott RW, Olson MF. LIM kinases: function, regulation and association with human disease. *J Mol Med* 2007; **85**: 555–68.

42 Hanna S, El-Sibai M. Signaling networks of Rho GTPases in cell motility. *Cellular Signalling* 2013; **25**: 1955–61.

43 Augoff K, Hryniewicz-Jankowska A, Tabola R. Invadopodia: clearing the way for cancer cell invasion. *Ann Transl Med* 2020; **8**: 902–902.

44 Sibony-Benyamini H, Gil-Henn H. Invadopodia: The leading force. *European Journal of Cell Biology* 2012; **91**: 896–901.

45 Guan X, Guan X, Dong C, Jiao Z. Rho GTPases and related signaling complexes in cell migration and invasion. *Experimental Cell Research* 2020; **388**: 111824.

46 Ridley AJ. Rho GTPase signalling in cell migration. *Current Opinion in Cell Biology* 2015; **36**: 103–12.

47 Hoffman L, Farley MM, Waxham MN. Calcium-Calmodulin-Dependent Protein Kinase II Isoforms Differentially Impact the Dynamics and Structure of the Actin Cytoskeleton. *Biochemistry* 2013; **52**: 1198–207.

48 Prudent J, Popgeorgiev N, Gadet R, Deygas M, Rimokh R, Gillet G. Mitochondrial Ca2+ uptake controls actin cytoskeleton dynamics during cell migration. *Sci Rep* 2016; **6**: 36570.

49 Wieder N, Greka A. Calcium, TRPC channels, and regulation of the actin cytoskeleton in podocytes: towards a future of targeted therapies. *Pediatr Nephrol* 2016; **31**: 1047–54.

50 Pozzi A, Yurchenco PD, Iozzo RV. The nature and biology of basement membranes. *Matrix Biology* 2017; **57–58**: 1–11.

51 Williams ED, Gao D, Redfern A, Thompson EW. Controversies around epithelial–mesenchymal plasticity in cancer metastasis. *Nat Rev Cancer* 2019; **19**: 716–32.

52 van Roy F. Beyond E-cadherin: roles of other cadherin superfamily members in cancer. *Nat Rev Cancer* 2014; **14**: 121–34.

53 Ramesh V, Brabletz T, Ceppi P. Targeting EMT in Cancer with Repurposed Metabolic Inhibitors. *Trends in Cancer* 2020; **6**: 942–50.

54 Davis FM, Azimi I, Faville RA, *et al.* Induction of epithelial–mesenchymal transition (EMT) in breast cancer cells is calcium signal dependent. *Oncogene* 2014; **33**: 2307–16.

55 Choe C, Ehrlich BE. The Inositol 1,4,5-Trisphosphate Receptor (IP_3R) and Its Regulators: Sometimes Good and Sometimes Bad Teamwork. *Sci STKE* 2006; **2006**. DOI:10.1126/stke.3632006re15.

56 Zalk R, Clarke OB, des Georges A, *et al.* Structure of a mammalian ryanodine receptor. *Nature* 2015; **517**: 44–9.

57 Anyatonwu GI, Estrada M, Tian X, Somlo S, Ehrlich BE. Regulation of ryanodine receptor-dependent calcium signaling by polycystin-2. *Proceedings of the National Academy of Sciences* 2007; **104**: 6454–9.

58 Sweeney HL, Holzbaur ELF. Motor Proteins. *Cold Spring Harb Perspect Biol* 2018; **10**: a021931.

59 Sharma RK, Parameswaran S. Calmodulin-binding proteins: A journey of 40 years. *Cell Calcium* 2018; **75**: 89–100.

60 Prevarskaya N, Skryma R, Shuba Y. Calcium in tumour metastasis: new roles for known actors. *Nat Rev Cancer* 2011; **11**: 609–18.

61 Chen Y-F, Chen Y-T, Chiu W-T, Shen M-R. Remodeling of calcium signaling in tumor progression. *J Biomed Sci* 2013; **20**: 23.

62 Ke C, Long S. Dysregulated transient receptor potential channel 1 expression and its correlation with clinical features and survival profile in surgical non-small-cell lung cancer patients. *Clinical Laboratory Analysis* 2022; published online Feb 2. DOI:10.1002/jcla.24229.

63 Ando H, Kawaai K, Bonneau B, Mikoshiba K. Remodeling of Ca 2+ signaling in cancer: Regulation of inositol 1,4,5-trisphosphate receptors through oncogenes and tumor suppressors. *Advances in Biological Regulation* 2018; **68**: 64–76.

64 Duan L, Wu R, Zou Z, *et al.* S100A6 stimulates proliferation and migration of colorectal carcinoma cells through activation of the MAPK pathways. *International Journal of Oncology* 2014; **44**: 781–90.

65 Wu R, Duan L, Cui F, *et al.* S100A9 promotes human hepatocellular carcinoma cell growth and invasion through RAGE-mediated ERK1/2 and p38 MAPK pathways. *Experimental Cell Research* 2015; **334**: 228–38.

66 Coticchia CM, Revankar CM, Deb TB, Dickson RB, Johnson MD. Calmodulin modulates Akt activity in human breast cancer cell lines. *Breast Cancer Res Treat* 2009; **115**: 545–60.

67 Brzozowski JS, Skelding KA. The Multi-Functional Calcium/Calmodulin Stimulated Protein Kinase (CaMK) Family: Emerging Targets for Anti-Cancer Therapeutic Intervention. *Pharmaceuticals* 2019; **12**: 8.

68 Predescu, Crețoiu, Crețoiu, *et al.* G Protein-Coupled Receptors (GPCRs)-Mediated Calcium Signaling in Ovarian Cancer: Focus on GPCRs activated by Neurotransmitters and Inflammation-Associated Molecules. *IJMS* 2019; **20**: 5568.

69 Pongs O, Lindemeier J, Zhu X, *et al.* Frequenin—A novel calcium-binding protein that modulates synaptic efficacy in the drosophila nervous system. *Neuron* 1993; **11**: 15–28.

70 Todd PAC, McCue HV, Haynes LP, Barclay JW, Burgoyne RD. Interaction of ARF-1.1 and neuronal calcium sensor-1 in the control of the temperature-dependency of locomotion in Caenorhabditis elegans. *Sci Rep* 2016; **6**: 30023.

71 Burgoyne RD. Neuronal calcium sensor proteins: generating diversity in neuronal Ca2+ signalling. *Nat Rev Neurosci* 2007; **8**: 182–93.

72 Bourne Y, Dannenberg J, Pollmann V, Marchot P, Pongs O. Immunocytochemical Localization and Crystal Structure of Human Frequenin (Neuronal Calcium Sensor 1). *Journal of Biological Chemistry* 2001; **276**: 11949–55.

73 Wang B, Boeckel GR, Huynh L, *et al.* Neuronal Calcium Sensor 1 Has Two Variants with Distinct Calcium Binding Characteristics. *PLoS ONE* 2016; **11**: e0161414.

74 Jeromin A, Muralidhar D, Parameswaran MN, *et al.* N-terminal Myristoylation Regulates Calcium-induced Conformational Changes in Neuronal Calcium Sensor-1. *Journal of Biological Chemistry* 2004; **279**: 27158–67.

75 Ames JB, Hendricks KB, Strahl T, Huttner IG, Hamasaki N, Thorner J. Structure and Calcium-Binding Properties of Frq1, a Novel Calcium Sensor in the Yeast *Saccharomyces cerevisiae*. *Biochemistry* 2000; **39**: 12149–61.

76 Weiss JL, Hui H, Burgoyne RD. Neuronal Calcium Sensor-1 Regulation of Calcium Channels, Secretion, and Neuronal Outgrowth. *Cell Mol Neurobiol* 2010; **30**: 1283–92.

77 Hui K, Fei G-H, Saab BJ, Su J, Roder JC, Feng Z-P. Neuronal calcium sensor-1 modulation of optimal calcium level for neurite outgrowth. *Development* 2007; **134**: 4479–89.

78 Nakamura TY, Jeromin A, Smith G, *et al.* Novel role of neuronal Ca2+ sensor-1 as a survival factor up-regulated in injured neurons. *Journal of Cell Biology* 2006; **172**: 1081–91.

79 McFerran BW, Graham ME, Burgoyne RD. Neuronal Ca2+ Sensor 1, the Mammalian Homologue of Frequenin, Is Expressed in Chromaffin and PC12 Cells and Regulates Neurosecretion from Dense-core Granules. *Journal of Biological Chemistry* 1998; **273**: 22768–72.

80 Pan C-Y, Jeromin A, Lundstrom K, Yoo SH, Roder J, Fox AP. Alterations in Exocytosis Induced by Neuronal Ca $^{2+}$ Sensor-1 in Bovine Chromaffin Cells. *J Neurosci* 2002; **22**: 2427–33.

81 Haynes LP, Thomas GMH, Burgoyne RD. Interaction of Neuronal Calcium Sensor-1 and ADP-ribosylation Factor 1 Allows Bidirectional Control of Phosphatidylinositol 4-

Kinase β and trans-Golgi Network-Plasma Membrane Traffic. *Journal of Biological Chemistry* 2005; **280**: 6047–54.

82 Haynes LP, Sherwood MW, Dolman NJ, Burgoyne RD. Specificity, Promiscuity and Localization of ARF Protein Interactions with NCS-1 and Phosphatidylinositol-4 Kinase-IIIβ. *Traffic* 2007; **8**: 1080–92.

83 Ng E, Varaschin RK, Su P, *et al.* Neuronal calcium sensor-1 deletion in the mouse decreases motivation and dopamine release in the nucleus accumbens. *Behavioural Brain Research* 2016; **301**: 213–25.

84 Fischer TT, Nguyen LD, Ehrlich BE. Neuronal calcium sensor 1 (NCS1) dependent modulation of neuronal morphology and development. *The FASEB Journal* 2021; **35**. DOI:10.1096/fj.202100731R.

85 Saab BJ, Georgiou J, Nath A, *et al.* NCS-1 in the Dentate Gyrus Promotes Exploration, Synaptic Plasticity, and Rapid Acquisition of Spatial Memory. *Neuron* 2009; **63**: 643–56.

86 Mun H-S, Saab BJ, Ng E, *et al.* Self-directed exploration provides a Ncs1-dependent learning bonus. *Sci Rep* 2015; **5**: 17697.

87 Kabbani N, Negyessy L, Lin R, Goldman-Rakic P, Levenson R. Interaction with Neuronal Calcium Sensor NCS-1 Mediates Desensitization of the D2 Dopamine Receptor. *J Neurosci* 2002; **22**: 8476–86.

88 Lian L-Y, Pandalaneni SR, Patel P, McCue HV, Haynes LP, Burgoyne RD. Characterisation of the Interaction of the C-Terminus of the Dopamine D2 Receptor with Neuronal Calcium Sensor-1. *PLoS ONE* 2011; **6**: e27779.

89 Nguyen LD, Petri ET, Huynh LK, Ehrlich BE. Characterization of NCS1–InsP3R1 interaction and its functional significance. *Journal of Biological Chemistry* 2019; **294**: 18923–33.

90 Schlecker C, Boehmerle W, Jeromin A, *et al.* Neuronal calcium sensor-1 enhancement of InsP3 receptor activity is inhibited by therapeutic levels of lithium. *J Clin Invest* 2006; **116**: 1668–74.

91 Nakamura TY, Jeromin A, Mikoshiba K, Wakabayashi S. Neuronal Calcium Sensor-1 Promotes Immature Heart Function and Hypertrophy by Enhancing Ca^{2+} Signals. *Circ Res* 2011; **109**: 512–23.

92 Schaad NC, De Castro E, Nef S, *et al.* Direct modulation of calmodulin targets by the neuronal calcium sensor NCS-1. *Proceedings of the National Academy of Sciences* 1996; **93**: 9253–8.

93 Grosshans HK, Fischer TT, Steinle JA, Brill AL, Ehrlich BE. Neuronal Calcium Sensor 1 is up-regulated in response to stress to promote cell survival and motility in cancer cells. *Mol Oncol* 2020; **14**: 1134–51.

94 Multani PK, Clarke T-K, Narasimhan S, *et al.* Neuronal calcium sensor-1 and cocaine addiction: A genetic association study in African-Americans and European Americans. *Neuroscience Letters* 2012; **531**: 46–51.

95 Piton A, Michaud JL, Peng H, *et al.* Mutations in the calcium-related gene IL1RAPL1 are associated with autism. *Human Molecular Genetics* 2008; **17**: 3965–74.

96 Handley MTW, Lian L-Y, Haynes LP, Burgoyne RD. Structural and Functional Deficits in a Neuronal Calcium Sensor-1 Mutant Identified in a Case of Autistic Spectrum Disorder. *PLoS ONE* 2010; **5**: e10534.

97 Dragicevic E, Poetschke C, Duda J, *et al.* Cav1.3 channels control D2-autoreceptor responses via NCS-1 in substantia nigra dopamine neurons. *Brain* 2014; **137**: 2287–302.

98 Koh PO, Undie AS, Kabbani N, Levenson R, Goldman-Rakic PS, Lidow MS. Up-regulation of neuronal calcium sensor-1 (NCS-1) in the prefrontal cortex of schizophrenic and bipolar patients. *Proceedings of the National Academy of Sciences* 2003; **100**: 313–7.

99 Torres KCL, Souza BR, Miranda DM, *et al.* Expression of neuronal calcium sensor-1 (NCS-1) is decreased in leukocytes of schizophrenia and bipolar disorder patients. *Progress in Neuro-Psychopharmacology and Biological Psychiatry* 2009; **33**: 229–34.

100 Boehmerle W, Splittgerber U, Lazarus MB, *et al.* Paclitaxel induces calcium oscillations via an inositol 1,4,5-trisphosphate receptor and neuronal calcium sensor 1-dependent mechanism. *Proceedings of the National Academy of Sciences* 2006; **103**: 18356–61.

101 Ibrahim EY, Ehrlich BE. Prevention of chemotherapy-induced peripheral neuropathy: A review of recent findings. *Critical Reviews in Oncology/Hematology* 2020; **145**: 102831.

102 Huehnchen P, van Kampen A, Boehmerle W, Endres M. Cognitive impairment after cytotoxic chemotherapy. *Neuro-Oncology Practice* 2020; **7**: 11–21.

103 Yang JD, Hainaut P, Gores GJ, Amadou A, Plymoth A, Roberts LR. A global view of hepatocellular carcinoma: trends, risk, prevention and management. *Nat Rev Gastroenterol Hepatol* 2019; **16**: 589–604.

104 Ally A, Balasundaram M, Carlsen R, *et al.* Comprehensive and Integrative Genomic Characterization of Hepatocellular Carcinoma. *Cell* 2017; **169**: 1327-1341.e23.

105 The ICGC/TCGA Pan-Cancer Analysis of Whole Genomes Consortium. Pan-cancer analysis of whole genomes. *Nature* 2020; **578**: 82–93.

106 Kutsenko A, Ladenheim MR, Kim N, *et al.* Increased Prevalence of Metabolic Risk Factors in Asian Americans With Hepatocellular Carcinoma. *Journal of Clinical Gastroenterology* 2017; **51**: 384–90.

107 Chaisaingmongkol J, Budhu A, Dang H, *et al.* Common Molecular Subtypes Among Asian Hepatocellular Carcinoma and Cholangiocarcinoma. *Cancer Cell* 2017; **32**: 57-70.e3.

108 Wu Y, Liu Z, Xu X. Molecular subtyping of hepatocellular carcinoma: A step toward precision medicine. *Cancer Communications* 2020; **40**: 681–93.

109 Djamai H, Berrou J, Dupont M, *et al.* Synergy of FLT3 inhibitors and the small molecule inhibitor of LIM kinase1/2 CEL_Amide in FLT3-ITD mutated Acute Myeloblastic Leukemia (AML) cells. *Leukemia Research* 2021; **100**: 106490.

110 Takemura M, Mishima T, Wang Y, *et al.* Ca2+/Calmodulin-dependent Protein Kinase IV-mediated LIM Kinase Activation Is Critical for Calcium Signal-induced Neurite Outgrowth. *Journal of Biological Chemistry* 2009; **284**: 28554–62.

111 Kanehisa M, Furumichi M, Sato Y, Ishiguro-Watanabe M, Tanabe M. KEGG: integrating viruses and cellular organisms. *Nucleic Acids Research* 2021; **49**: D545–51.

112 Paquette J, Tokuyasu T. EGAN: exploratory gene association networks. *Bioinformatics* 2010; **26**: 285–6.

7. Appendix

7.1 List of Figures

8. Pre-Released Results

The findings discussed in this study were published in the following scientific journals:

Daniel Schuette, Lauren M. Moore, Marie E. Robert, Tamar H. Taddei, and Barbara E. Ehrlich: *Hepatocellular Carcinoma Outcome is Predicted by Expression of Neuronal Calcium Sensor 1*. Cancer Epidemiol Biomarkers Prev. Published May 2018. DOI: 10.1158/1055-9965.EPI-18-0167.

Jonathan E. Apasu, **Daniel Schuette**, Ryan LaRanger, Julia A. Steinle, Lien D. Nguyen, Henrike K. Grosshans, Meiling Zhang, Wesley L. Cai, Qin Yan, Marie E. Robert, Michael Mak, and Barbara E. Ehrlich: *Neuronal calcium sensor 1 (NCS1) promotes motility and metastatic spread of breast cancer cells in vitro and in vivo*. FASEB J. Published April 2019. DOI: 10.1096/fj.201802004R.

Research Article

Cancer Epidemiology, Biomarkers & Prevention

Hepatocellular Carcinoma Outcome Is Predicted by Expression of Neuronal Calcium Sensor 1

Daniel Schuette[1], Lauren M. Moore[1], Marie E. Robert[2], Tamar H. Taddei[3], and Barbara E. Ehrlich[1]

Abstract

Background: Hepatocellular carcinoma (HCC) is the second leading cause of cancer-related death worldwide. There is an urgent demand for prognostic biomarkers that facilitate early tumor detection, as the incidence of HCC has tripled in the United States in the last three decades. Biomarkers to identify populations at risk would have significant impact on survival. We recently found that expression of Neuronal Calcium Sensor 1 (NCS1), a $Ca2^+$-dependent signaling molecule, predicted disease outcome in breast cancer, but its predictive value in other cancer types is unknown. This protein is potentially useful because increased NCS1 regulates $Ca2^+$ signaling and increased $Ca2^+$ signaling is a hallmark of metastatic cancers, conferring cellular motility and an increasingly aggressive phenotype to tumors.

Methods: We explored the relationship between NCS1 expression levels and patient survival in two publicly available liver cancer cohorts and a tumor microarray using data mining strategies.

Results: High NCS1 expression levels are significantly associated with worse disease outcome in Asian patients within these cohorts. In addition, a variety of $Ca2^+$-dependent and tumor growth-promoting genes are transcriptionally coregulated with NCS1 and many of them are involved in cytoskeleton organization, suggesting that NCS1 induced dysregulated $Ca2^+$ signaling facilitates cellular motility and metastasis.

Conclusions: We found NCS1 to be a novel biomarker in HCC. Furthermore, our study identified a pharmacologically targetable signaling complex that can influence tumor progression in HCC.

Impact: These results lay the foundation for using NCS1 as a prognostic biomarker in prospective cohorts of HCC patients and for further functional assessment of the characterized signaling axis. *Cancer Epidemiol Biomarkers Prev; 27(9); 1091–100. ©2018 AACR.*

Introduction

Hepatocellular carcinoma (HCC) is one of the deadliest cancer types worldwide (1), with rapidly increasing rates in the United States (2, 3). Currently, options to cure or palliate HCC are limited to resection, transplantation, and ablative and transarterial therapies, with therapeutic choices dictated by both tumor burden and the extent of hepatic dysfunction. There is only one FDA-approved first-line, palliative systemic chemotherapeutic agent, an oral tyrosine kinase inhibitor (sorafenib). This treatment is reserved for patients who have failed or progressed after local therapies, offering an overall survival advantage of 3 months with a significant adverse side effect profile (4). To develop and optimize new treatment modalities for HCC, novel biomarkers are needed that can predict tumor aggressiveness and identify druggable targets that can be exploited to create innovative therapies.

Calcium is long known to be a major regulator of cell-cycle progression and cellular proliferation, events promoted by growth factors that often cause oscillatory patterns of Ca^{2+} release from ER stores and Ca^{2+} entry from the extracellular space (5–7). Furthermore, recent clinical and basic research evidence implicates a Ca^{2+}-driven pro-metastatic phenotype in aggressive tumors with an unfavorable prognosis (8–10). To date, only one component of Ca^{2+}-signaling pathways has been proposed as a potential biomarker for HCC. High expression of S100 Ca^{2+}-binding proteins is reported to confer an aggressive phenotype in undifferentiated liver cancers (11–14). Although less well characterized, other members of the Ca^{2+}-signaling cascade have been implicated in cancer progression (15).

Neuronal Calcium Sensor 1 (NCS1) is a clinically validated prognostic biomarker in two independent breast cancer cohorts, that is closely related to states of dysregulated Ca^{2+}-signaling (10). NCS1, a member of the calmodulin superfamily of EF-hand Ca^{2+}-sensing proteins, is involved in various cellular processes, including exocytosis (16), regulation of voltage-gated Ca^{2+}-channels, neuroplasticity (17), and calmodulin-mediated signaling (18). NCS1 interacts with inositol 1,4,5-triphosphate receptor type 1 (InsP3R1) and leads to an increase in InsP3-dependent Ca^{2+}-release (19), especially in an overexpression scenario (20, 21). NCS1 also is upregulated in injured neurons, acting as a survival factor via activation of PI3K/AKT pathway (22). These functional properties and its expression in different extra-neuronal tissues (23–26) together with its likely role in breast cancer development make NCS1 a possible contributor to carcinogenesis in other tumor types as well.

[1]Department of Pharmacology, Yale University, New Haven, Connecticut. [2]Department of Pathology, Yale University, New Haven, Connecticut. [3]Department of Medicine (Digestive Diseases), Yale University, New Haven, Connecticut.

Note: Supplementary data for this article are available at Cancer Epidemiology, Biomarkers & Prevention Online (http://cebp.aacrjournals.org/).

Current address for L.M. Moore: Memorial Sloan Kettering Cancer Center, 327 E. 64th Street, NY 10065.

Corresponding Author: Barbara E. Ehrlich, 333 Cedar Street, Yale University, New Haven, CT 06520-8066. Phone: 203-737-1158; Fax: 203-737-2027. E-mail: barbara.ehrlich@yale.edu

doi: 10.1158/1055-9965.EPI-18-0167

To investigate the possible role of NCS1 in Ca^{2+}-mediated tumor progression and metastasis in HCC, we analyzed The Cancer Genome Atlas (TCGA) Liver Hepatocellular Carcinoma (LIHC) dataset to determine whether there is an association of NCS1 with patient survival and whether NCS1 can distinguish among patients, either by sub-population or etiologic risk factor. In addition, we built a regression model to test for significant coexpression of NCS1 using the approximately 60,000 RNA-sequenced transcripts included in the TCGA LIHC dataset. Using information from the regression model, we identified pathways involved in Ca^{2+} and NCS1 signaling that influence tumor progression and can be pharmacologically manipulated.

Materials and Methods

Data download

The results shown here are in part based upon data generated by the TCGA Research Network: http://cancergenome.nih.gov/. TCGA LIHC, breast cancer (BRCA), and lung cancer (LUAD and LUSC) expression data and clinical annotations were download from the NIH's Genomic Data Commons (GDC) Data Portal (https://portal.gdc.cancer.gov) on October 10, 2017. Plain text files with FPKM values for 60 483 transcripts per patient were joined with corresponding clinical annotations and gene names were added using unique ENSG identifiers (ensembl.org, GRCh38.p11). NCS1 and LIMK1 expression values and clinical annotations related to the International Cancer Genome consortium (ICGC) LIRI-JP liver cancer cohort were downloaded from the ICGC data portal (https://icgcportal.genomics.cn) on February 22, 2018. All data transformation and analyses were performed with R Statistical Programming Language, Version 3.4.0 (2017-04-21; ref. 27). Additional information regarding sample processing, patient characteristics, data acquisition and global mutational and expressional analyses are available with The Cancer Genome Atlas Research Network's publications of these datasets (28–31). Data for NCS1, GAPDH, RPS18, HPRT1 and ACTB expression levels in various tissues that lack HCC (assumed to be healthy for the purposes of this study) were accessed through the websites of The Genotype-Tissue Expression (GTEx) Project (https://www.gtexportal.org/home/) as well as The Human Protein Atlas (HPA; https://www.proteinatlas.org) (both on November 1, 2017). Pre-processed gene expression data of 1,019 cancer cell lines are publicly available through Broad Institute's Cancer Cell Line Encyclopedia (CCLE; https://portals.broadinstitute.org/ccle) and were downloaded on January 10, 2018.

Bioinformatics and statistical analyses

The between-group comparisons of overall survival were performed by means of two-sided log-rank tests stratified according to NCS1 (<75% vs. $\geq$ 75%), WDR5 (<80% vs. $\geq$ 80) and LIMK1 (<60% vs. >60%) expression levels. Cutoff values for dichotomizing continuous expression values to "high" and "low" were derived from receiver operating characteristics (ROC) curves using Youden's J statistic. A Cox proportional-hazards model that included dichotomized NCS1, LIMK1, and WDR5 expression as covariates was used to estimate hazard ratios (HRs) and their associated 95% confidence intervals (CIs). The Kaplan–Meier method was used to estimate survival curves and a log-rank test to compare survival between distinct expression subgroups. Survival plots and forest plots were generated using the "survminer" R package (32). In all analyses, patient samples were excluded whenever survival data or expression values were missing (<10% per cohort and analysis).

To assess transcriptional coregulation of the 60,482 transcripts with NCS1 expression in LIHC, BRCA, LUAD, and LUSC datasets, simple linear regression analysis was performed. *P* values derived from these analyses were corrected using Bonferroni's method and top hits were identified by means of corrected *P* values. We pre-specified a threshold for Pearson's correlation coefficient of 0.6 or higher to indicate a strong correlation, mainly to reduce the false positive rate (33). Again, a univariate linear regression model was used to compute the relationship between NCS1 and LIMK1 or WDR5 in the TCGA, ICGC, and CCLE datasets.

Exploratory Gene Association Networks (EGAN; ref. 34) software was used to combine NCS1-correlated genes and database-derived gene and pathway annotations into meaningful network plots. A list of 40 genes, comprising the top 10 hits from all 4 datasets, was examined for overlaps with pathways from the Molecular Signature Database (MSigDB, http://software.broadinstitute.org/gsea/msigdb) and by means of EGAN software. Results with an FDR $q < 0.05$ were called significant and listed as relevant. Welch's two sample *t* test was used to test for statistical differences of sample means if not otherwise specified and Fisher's exact test was used to analyze contingency tables.

Liver cancer tissue array

A commercially available HCC microarray with 49 cases (2 cores per case, 41 tumors with matched non-neoplastic adjacent tissue, 6 tumors without matched non-neoplastic tissue, and 2 normal liver tissues without corresponding tumors) was purchased from US Biomax, Inc. (OD-CT-DgLivT10-024, HLiv-HCC180Bch-01). Immunofluorescence staining for NCS1 and arginase was performed and automated quantitative analysis (AQUA) with arginase as a marker for tumor tissue compared with stromal tissue was used to quantify NCS1 protein levels in tumors and adjacent non-neoplastic tissues, as previously described (10). Biochemical indicators (AFP, CA19-9, CEA, hepatitis B/C markers, Creatinine, BUN) and tumor stage data are available on the supplier's website.

Results

Tissue NCS1 expression increases during HCC carcinogenesis

To assess physiological NCS1 expression in normal liver tissue from healthy individuals, we explored two databases; GTEx Project and HPA. Analysis of both of these datasets suggests very low overall NCS1 levels in healthy human liver (mean NCS1 expression levels derived from RNA-sequencing specified as 0.9 TPM and 0.7 RPKM in 10 and 119 specimens in the HPA and GTEx datasets, respectively). Furthermore, when compared with other organs, liver expression levels rank last and second to last among 31 and 36 analyzed tissues in the HPA and GTEx datasets, respectively. Because interexperimental comparison of expression units is usually not possible, we calculated the ratio of NCS1 to the housekeeping gene β-actin (ACTB) in HPA, GTEx, and TCGA LIHC datasets (Fig. 1A). The ratio of NCS1 to ACTB was 1.7- and 1.4-fold higher in cancerous tissue ($P < 0.01$ for the comparison of TCGA vs. GTEx and TCGA vs. HPA, respectively). To validate the choice of ACTB for normalization, three additional housekeeping genes (HPRT1, GAPDH, and RPS1) were used to normalize the NCS1 levels (Supplementary Fig. S1). An increase in NCS1 expression levels in the HCC samples was observed with all

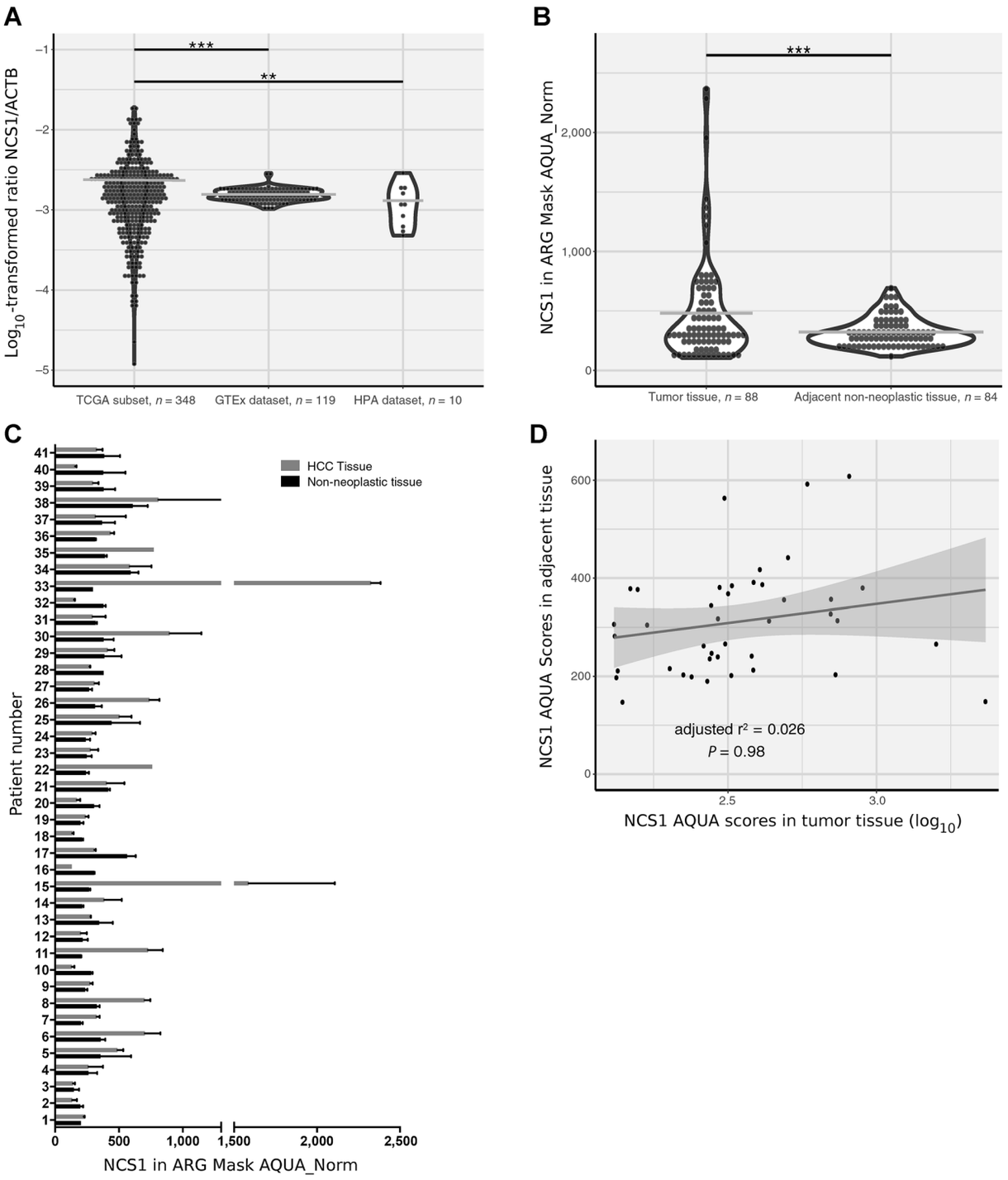

Figure 1.

NCS1 expression in non-neoplastic and cancerous tissue. **A,** Dot plot showing the ratio of NCS1 to the housekeeping gene ACTB on a $\log_{10}$-transformed scale for 3 different datasets. ***, $P < 0.0001$; **, $P < 0.001$ and horizontal lines indicate sample means. Violin plots visualize the overall data distribution per sample. Data on NCS1 and ACTB expression are only available for a subset of TCGA samples. **B,** Dot plot showing AQUA scores for NCS1 in tumor tissue compared with adjacent non-neoplastic tissue. Data are derived from a tumor microarray and a "tumor mask" was generated using of arginase (ARG) signal to discriminate tumorous from stromal tissue compartments. A paired *t* test was used to assess group differences. **C,** Bar plot showing AQUA scores for tumors and adjacent normals of 41 patients. Error bars represent standard deviations of $n = 2$ cores per sample and bars represent sample means. **D,** Scatter plot for NCS1 AQUA scores in tumor tissue versus matched adjacent non-neoplastic tissues. Trend line with 95% CI is based on a simple linear regression model to visualize random distribution of the data and summary statistics of that regression model are added to the plot.

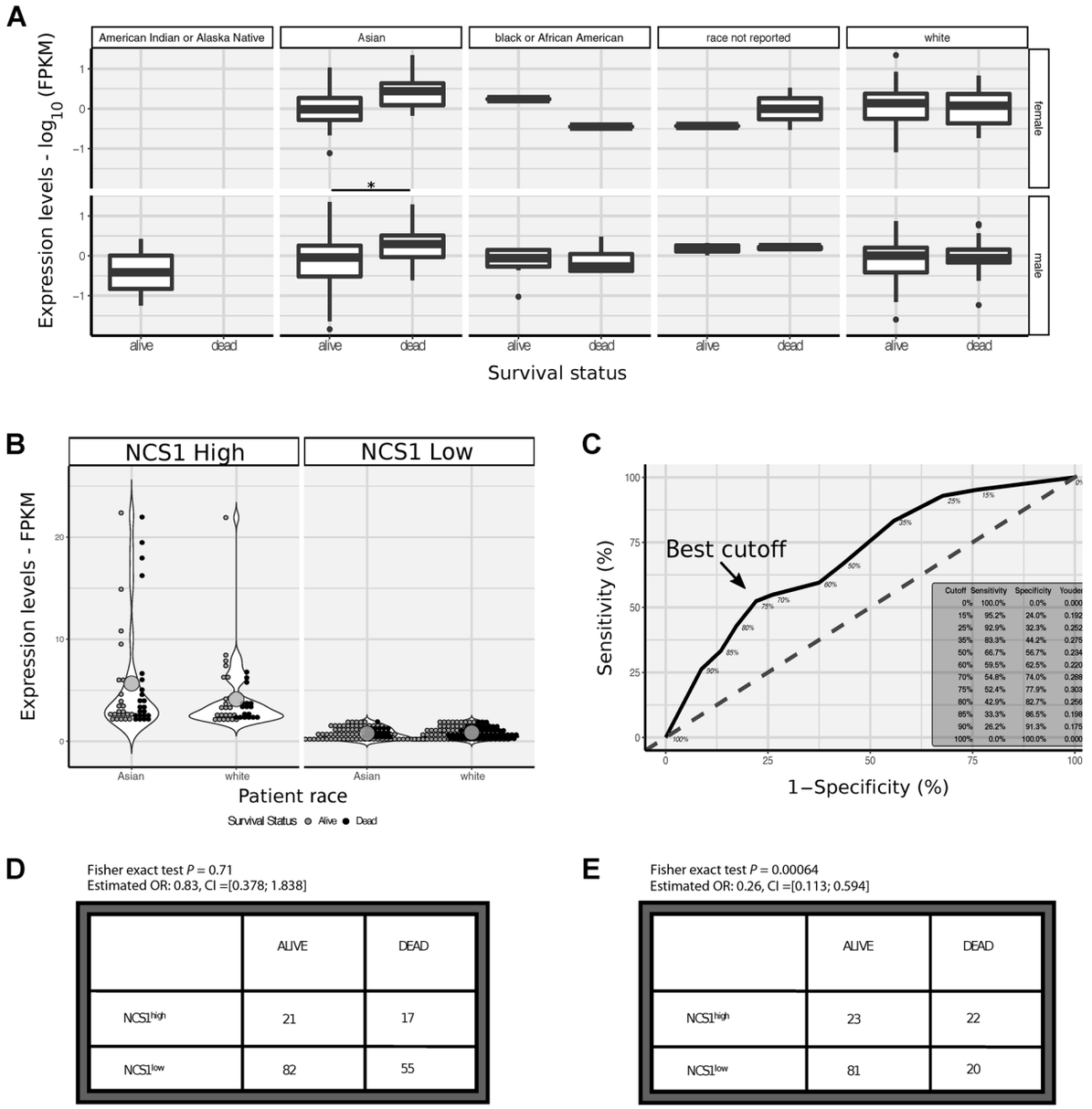

Figure 2.

NCS1 expression and patient survival. **A,** Boxplots showing $\log_{10}$-transformed, continuous NCS1 expression levels for male and female patients in rows and different races in columns. Adjacent boxplots partition respective patient populations by survival status. See Supplementary Table S1 for additional information on sample size. *, indicates corrected $P < 0.05$ in a two-sided t test. **B,** Dot plots comparing mean (represented by large dots) NCS1 expression levels for $NCS1^{high}$ and $NCS1^{low}$ Asian and white patients. Violin plots visualize overall data distribution. Shades of gray represent survival status of patients. Two-sided t test $P = 0.056$ for comparison of NCS1 expression levels in Asian versus white patients (estimated means 2.28 vs. 1.59, respectively). **C,** Receiver operating characteristic curve showing the optimum cutoff for dichotomizing NCS1 expression in Asian patients to "high" and "low" to be 75% (75% of patients categorized as "low," 25% as "high"; indicated by an arrow). Inset in lower right corner lists sensitivity, specificity, and Youden's J statistic for different cutoffs. **D** and **E,** Contingency tables showing NCS1 and survival status for white and Asian patients, respectively. P values were calculated using Fisher's exact test, ORs, and 95% CIs are listed above tables.

housekeeping genes. These results suggest NCS1 levels increase in liver tissue during HCC development.

To further examine this hypothesis, a commercially available microarray composed of HCC samples and adjacent non-neoplastic tissues was analyzed using immunofluorescence to calculate AQUA scores. Matched adjacent non-neoplastic tissues were available for most tumor samples (41/47) on the array. A significant ($P < 0.0001$) upregulation of NCS1 was observed in tumors (Fig. 1B), with 59% (24/41) of them showing increased NCS1 AQUA scores compared with matched non-neoplastic samples (Fig. 1C). However, in all of the samples, the levels of NCS1 in the non-neoplastic tissue is low and there is a very small

range, suggesting that baseline NCS1 will not be a predictor for development of HCC and that high baseline NCS1 expression cannot be a prerequisite for the development of HCC. This is more clearly shown by the relationship between AQUA scores in tumors and non-neoplastic samples (Fig. 1D). Each data point is the expression of NCS1 in tumors and non-neoplastic samples in the same patient and the scatter of the data points show that there is no correlation. This relationship suggests that baseline NCS1 levels do not predict the expression level of NCS1 in the tumor samples and provides further evidence that increased NCS1 expression is associated with tumor development. An analysis of the limited clinical annotations available for the array showed no association of NCS1 AQUA scores in tumor tissue with either tumor stage (Supplementary Fig. S2B), hepatitis B/C status, tumor markers (CEA, CA19-9, AFP) or any of the patient characteristics (age and gender). No additional information on the spatial relationship between tumor samples and non-neoplastic adjacent tissues were available for analysis.

NCS1 levels predict survival status and time to death in a subgroup of Asian patients

To test whether NCS1 levels correlate with tumor stage and outcome in the TCGA cohort of liver cancer patients, we examined the relationship between NCS1 expression measured in FPKM units and clinical tumor stage for 377 patients. Although advanced tumors did not show increased NCS1 expression compared with early-stage tumors in this cohort (Supplementary Fig. S2A), in the subgroup of Asian patients who died, average NCS1 expression was significantly increased compared with the survivors (t-test corrected $P < 0.05$ for male Asian patients, Fig. 2A). In addition, Asian patients had a higher mean NCS1 expression than white patients (t test $P = 0.056$) and a significantly ($P < 0.01$) smaller proportion of $NCS1^{low}$ Asian patients died during the course of their disease (21.4% vs. 39.0% for Asian and white patients, respectively, Fig. 2B), irrespective of tumor stage. This comparison suggests a protective effect of low NCS1 expression in $NCS1^{low}$ Asian patients. Differences in the expression profiles of proteins associated with HCC among races has recently been described (35). With respect to Ca^{2+}-signaling pathways, indel mutations in ryanodine receptors (RYRs; intracellular Ca^{2+} channels) were identified in Thai patients in this study (35). Because the number of subjects from races other than Asians and whites constitute only a small part of the overall sample (Supplementary Table S1), they were excluded from further analyses.

In the next analysis, we examined the prognostic value of dichotomized NCS1 expression levels (to $NCS1^{high}$ and $NCS1^{low}$) with regard to patient survival at the last follow-up and over time. To explore the optimum cutoff for dichotomization of continuous FPKM values, we created a receiver operating characteristics (ROC) curve by calculating sensitivity and specificity for a range of different cutoffs and calculated Youden's J statistic to capture the performance of our binary test (Fig. 2C). As a result, we categorized 25% of patients as $NCS1^{high}$ and 75% as $NCS1^{low}$.

When applying this cutoff value to the survival status of Asian patients (i.e., patients being either dead or alive at the time of last follow-up), the estimated odds ratio of 0.26 shows a significant (Fisher's exact test $P < 0.001$) association of high NCS1 expression levels with an unfavorable disease outcome (Fig. 2E). However, the relationship between NCS1 expression and prognosis is not true for white patients (Fig. 2D), confirming the result of our prior analysis.

We next estimated survival curves via the Kaplan–Meier method and applied a Cox proportional-hazards model with NCS1 as a single covariate to calculate HRs for all patients in the TCGA LIHC cohort (Fig. 3A), as well as race-stratified for the subgroup of Asian (Fig. 3B) and for the subgroup of white patients (Fig. 3C). With this approach, Asians showed a significantly higher probability of death if categorized as $NCS1^{high}$ (HR, 3.5; $P < 0.0001$), whereas the time to death in white patients was independent of their NCS1 status (HR, 0.89; $P = 0.68$). NCS1 status was also significantly associated with worse outcome in the Kaplan–Meier analysis of all patients (HR, 1.7; $P = 0.006$), although with a hazard ratio closer to 1 than the ratio calculated for Asian patients only.

NCS1 status predicts survival in an independent cohort of Japanese HCC patients

To validate the strong relationship between high NCS1 expression and survival of Asian patients in the TCGA LIHC cohort, we then examined the International Cancer Genome Consortium (ICGC) LIRI-JP cohort (36) that comprises 231 HCC samples from Japanese patients. After dichotomizing continuous NCS1 expression levels in $NCS1^{high}$ and NCS^{low} as described above, we again found that high expression was significantly associated with worse patient survival over time (Fig. 3D; with an unadjusted HR, 1.96; $P = 0.039$).

LIMK1 and WDR5 are transcriptionally coregulated with NCS1

Because the exact signaling pathway that is influenced by NCS1 expression in tumor cells remains to be elucidated, we performed simple linear regression analyses of NCS1 with 60 483 RNA-sequenced transcripts from the TCGA LIHC dataset to assess transcriptional coregulation of certain transcripts with NCS1. After correcting for multiple hypothesis testing, a total of 54 genes were significantly ($P < 10^{-30}$ and Pearson's correlation coefficient above the pre-specified threshold of 0.6) and positively correlated with NCS1 expression (Supplementary Fig. S3; Supplementary Table S2). LIM Domain Kinase 1 (LIMK1) was the most significantly coexpressed gene and remarkably, LIMK1 stands out, separate from all the other genes that are associated with NCS1 (Supplementary Fig. S3 and Supplementary Fig. S4A, NCS1 vs. LIMK1 Pearson's $r = 0.76$, $P < 0.0001$). We further validated the strong coexpression by exploring the relationship of NCS1 and LIMK1 in the ICGC LIRI-JP cohort (Supplementary Fig. S4B, Pearson's $r = 0.72$, $P < 0.0001$).

With this information, we constructed a coexpression network (37) using EGAN (Fig. 4A; ref. 34) software. We found cytoskeleton organization to be the dominant pathway in the derived network. To further minimize bias and improve robustness of the approach, we analyzed three additional TCGA cohorts (LUAD, LUSC, and BRCA; Supplementary Table S2 for top hits and Supplementary Fig. S5 for gene association networks) using the same methods and included only the 10 most significant results from each cohort in our pathway analysis.

In this expanded cohort, two genes occurred among the top 10 NCS1-associated genes in at least two of four samples, namely LIMK1 (overlapped between two datasets) and WD Repeat Domain 5 (WDR5, overlapped between three datasets). We calculated a Cox proportional-hazards model that includes

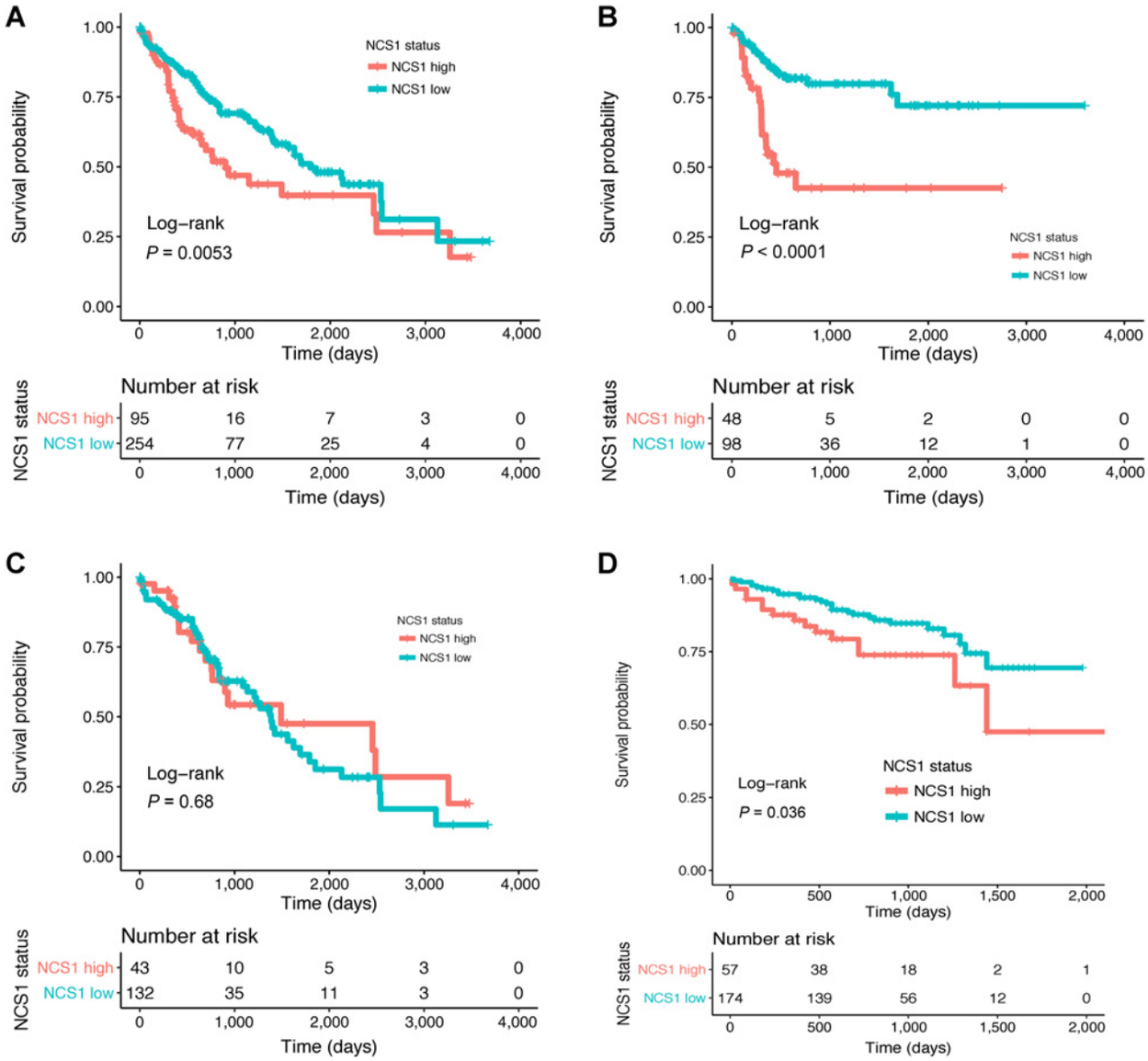

Figure 3.

NCS1 status and patient survival. **A,** Kaplan–Meier plot showing survival probability for 349 patients from the TCGA LIHC cohort. HR, 1.7 ($P = 0.006$; 95% CI, 1.2–2.4). **B,** Kaplan–Meier plot showing survival probability for $n = 146$ Asian patients from the TCGA LIHC cohort. HR, 3.5 ($P < 0.0001$; 95% CI, 1.9–6.5). **C,** Kaplan–Meier plot showing survival probability for $n = 175$ white patients from the TCGA LIHC cohort. HR, 0.89 ($P = 0.68$; 95% CI, 0.52–1.5). **D,** Kaplan–Meier plot showing survival probability for 231 patients from the ICGC LIRI-JP cohort. HR, 1.96 ($P = 0.039$; 95% CI, 1.03–3.7).

dichotomized NCS1, LIMK1, and WDR5 expression as covariates and adjusts for patient age and gender to investigate the prognostic significance of these three NCS1 associated genes in the TCGA LIHC cohort. Although not all of the calculated hazard ratios become significant due to the relatively small number of events, all analyses predicted an increased risk of death in patients with high expression of the respective genes compared with patients with low expression (Fig. 4B; Supplementary Fig. S6A shows the respective forest plot for white patients). These effects were stable and independent of patient age or gender. In addition, we examined the genes that overlap with pathways from the Molecular Signature Database (MSigDB). Again, we found that the genes identified in our analysis are related to either Ca^{2+}-dependent signaling pathways (cell-cycle progression, cytoskeleton organization), neurogenesis or cancer-related pathways (Supplementary Fig. S6B).

We also examined Broad Institute's Cancer Cell Line Encyclopedia (CCLE) dataset that comprises RNA sequencing derived expression data of 1,019 cell lines to further test and potentially validate the positive correlation between NCS1 and LIMK1 or WDR5. Consistent with our pathway analysis, the relationship between NCS1 and LIMK1 is observed in breast and liver cancers, but not in cell lines derived from hematological malignancies that do not require increased

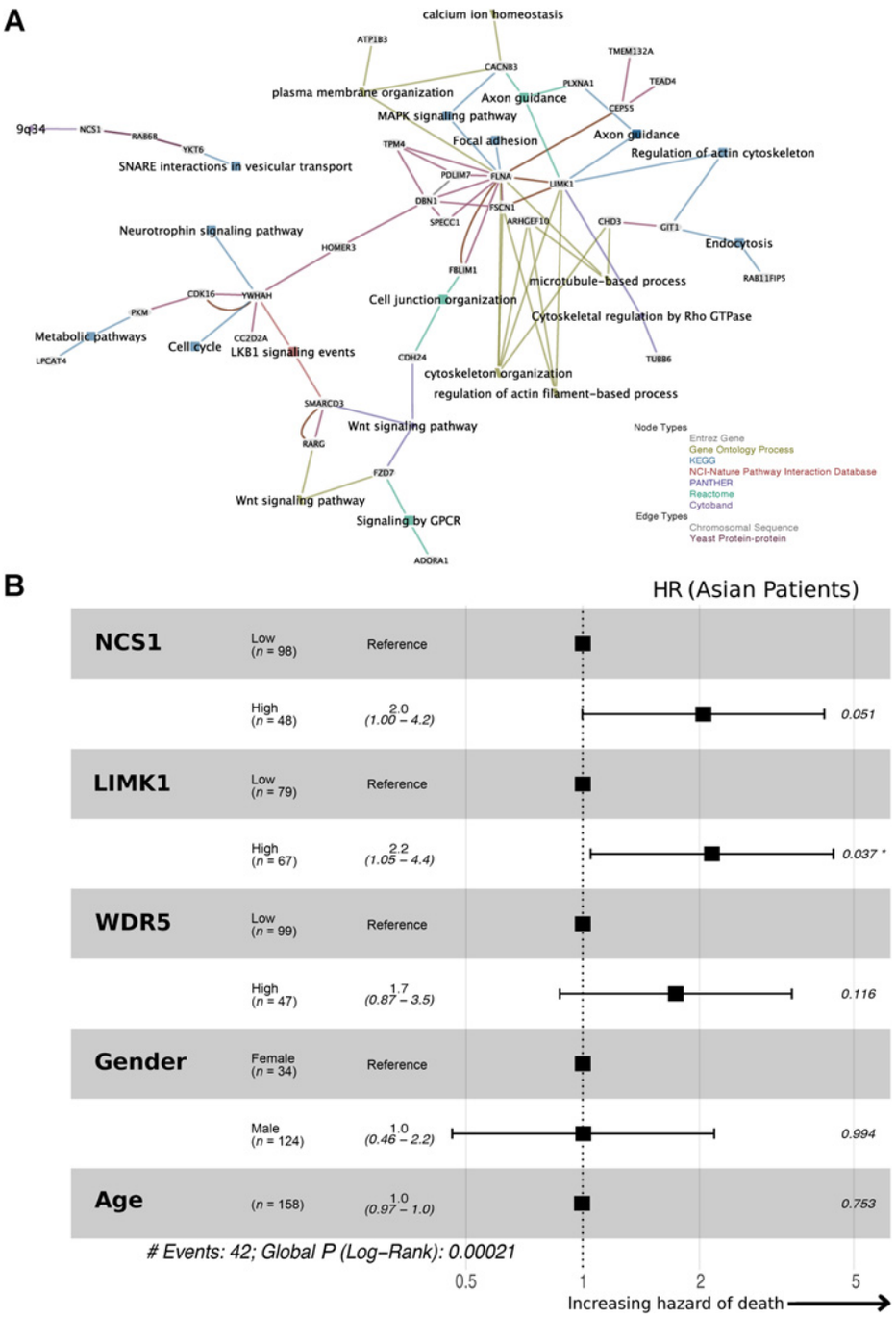

Figure 4.

NCS1-associated signaling pathways in HCC. **A,** Coexpression network constructed from 54 NCS1 associated genes using EGAN software; 34 genes are actually part of the network. A legend in the lower right corner explains node and edge types. To not introduce bias, all pathways that comprise at least 2 of the 54 genes are included in the network. **B,** Forest plot showing HRs derived from a Cox proportional-hazards model that includes dichotomized NCS1, LIMK1 and WDR5 expression, patient age, and gender as covariates to predict survival of Asian TCGA LIHC patients. Dichotomization cutoffs are chosen according to ROC curves. Number of events = 42, $P = 0.0002$ for all covariates together.

motility and cytoskeleton remodeling for metastasis. In contrast, NCS1 and WDR5 did not show a significant correlation in the CCLE dataset, independent of cancer type (Supplementary Fig. S7A and S7B).

Discussion

In this study, we systematically examined the prognostic role of NCS1 and transcriptionally associated genes in a liver cancer cohort from a publicly available database. Interestingly, healthy liver tissue exhibited lower overall NCS1 levels compared with HCC, suggesting an upregulation of NCS1 during tumorigenesis. We were able to validate this finding by using a tissue microarray where 59% of tumors harbored NCS1 levels (as assessed by a quantitative immunofluorescence technique) that were increased compared with the matched non-neoplastic tissues. We did not see a correlation between NCS1 levels in these matched adjacent non-neoplastic tissues and NCS1 levels in the respective tumor samples. This result supports our hypothesis that NCS1 is upregulated during carcinogenesis, in a manner independent of basal

levels in the healthy organ or tumor-adjacent parenchyma. We suggest that NCS1 expression is a fixed, tumor dependent phenomenon that is associated with risk factors or concomitant liver diseases, irrespective of stage at diagnosis.

By correlating RNA-sequencing–based expression to clinical outcome measures, specifically survival status of patients at the end of follow-up and time to death, we demonstrated a significantly worse prognosis for Asian patients with high NCS1 expression compared with Asians with low NCS1 expression. We validated this finding by investigating an additional, independent cohort of Asian HCC patients. Although we found NCS1 to be predictive of survival in an analysis of all TCGA samples, we hypothesize that the observed effect is mainly driven by the subpopulation of Asian patients because we did not see an association of NCS1 with survival for white patients. In addition to these analyses, we identified an associated signaling network whose central components further improved survival predictions. The expression pattern of these genes suggests a path for the development of prognostic biomarkers and potential targeted therapies.

One possible cause for the observed race-specific differences regarding survival might be the overall higher expression of NCS1 among Asian cancer patients. This differential expression may be caused by hepatocellular carcinoma-associated risk factors, including hepatitis or alcohol exposure, although a mechanistic explanation is beyond the scope of this study. Nevertheless, it is known that HCCs differ between Asian and white patients in terms of genomic properties (35) and with respect to pro-carcinogenic risk factors (38). In this regard, our study adds to an increasing body of literature investigating possible contributors to these phenomena. Importantly, our study suggests a specific cellular mechanism, dysregulated Ca^{2+} signaling, as a hallmark of HCC in a subgroup of patients.

To facilitate a better understanding of the biology of tumors expressing high levels of NCS1, we investigated additional cancer datasets, two lung cancer and one breast cancer datasets, for significant coregulation of NCS1 with other transcripts. We found a range of pro-oncogenic genes to be highly expressed in $NCS1^{high}$ patients and identified the associated pathways to be cytoskeleton organization, neurogenesis and cell-cycle progression. Furthermore, most of the identified genes are involved in cancer- and metastasis-related pathways, underscoring the validity of the analysis.

Two genes appeared to be NCS1-associated in at least two of the four examined TCGA datasets (WDR5 and LIMK1). WDR5 is a protein shown to be Ca^{2+} sensitive in amphibians (39) and it has a critical role in recruiting the highly oncogenic transcription factor MYC (40) and epigenetic modifiers MLL1–4 (41, 42) to chromatin (43). This study is the first time WDR5 has been proposed to be associated with NCS1 as a crucial (dys)regulator of intracellular Ca^{2+}-signaling. The WDR5/MLL complex has been suggested as a contributor to an unfavorable disease outcome in HCC (44) and MLL4 is a known target of HBV integration, especially in Chinese patients (45). However, WDR5 ranks only among the top 500 genes when analyzing the TCGA LIHC dataset. To include WDR5 as a critical component of tumorigenesis would require a robust validation of a functional role of WDR5 beyond mere association, especially as it is located in close chromosomal proximity to NCS1 and was not correlated in an analysis of RNA sequencing data from the CCLE.

LIMK1 is a promising therapeutic target that was previously studied with regard to metastasis and appeared prominently in our analyses of TCGA and CCLE datasets. Cellular motility, a hallmark of metastatic cancers, is mainly facilitated via actin polymerization (46) and LIMK1 is a key regulator of this process (47). In addition, Ca^{2+}-dependent LIMK1 activation was observed in neuronal outgrowth (48). The second most significantly coexpressed gene in the analyzed liver cancer cohort is ARHGEF10, a RhoA guanine nucleotide exchange factor that acts upstream of LIMK1 (49). From the potential functional combination of these proteins along with components of our coexpression network (Fig. 4A), we hypothesize an increased activation of the RhoA—Rho-associated protein kinase (ROCK)—LIMK1 signaling axis in tumor cells exhibiting increased NCS1 levels (50). This functional complex confers motility and allows tumor cells to interact with the stroma and microenvironment, and expressional upregulation would ultimately lead to decreased patient survival. Because potent inhibitors of LIMK1 have been developed that can reduce cellular motility *in vitro* (51), LIMK1 is a potential clinical target in advanced HCC, possibly in combination with inhibitors that address additional components of a larger signaling network. Furthermore, our results suggest that the NCS1/LIMK1 signaling network can be modeled using cancer cell lines.

Other Ca^{2+}-dependent pathways that have been causally related to HCC development (e.g., the lysophosphatidic acid pathway; ref. 52) may be directly or indirectly associated with NCS1 expression. However, these pathways were not identified in the cohort included in this study.

The main limitations of this study are the relatively small number of Asian patients in the TCGA LIHC cohort, the focus on pre-processed RNA-sequencing as the primary measure of protein expression, and the limited availability of patients' past medical histories. Our hypothesis that NCS1 increases during hepatocarcinogenesis is based on a TMA with HCC samples and non-neoplastic adjacent tissues. To test this hypothesis, longitudinal studies are required to explore the role of NCS1 during the evolution of HCC in greater depth. This is especially import with regard to recent evidence suggesting that liver tissue adjacent to a primary liver tumor might have expression patterns or phenotypes different from normal hepatocytes (53).

Moreover, the excellent overall survival rate of about 65% after 10 years in the TCGA study suggests a bias in this cohort toward patients that were treated with a curative intention and thus had on average a longer survival than usually observed with HCC. Nevertheless, our study points to cytoskeleton remodeling, possibly facilitated by an interaction of NCS1 and the RhoA/ROCK/LIMK1 pathway, as an important determinant of aggressive HCC. The question whether disruption of this pathway applies only to a distinct subgroup of patients or to all HCC patients with NCS1 levels beyond a certain cutoff value, will be addressed in subsequent studies.

In summary, using a database-focused proof-of-concept study to analyze the predictive capacity of the multifunctional Ca^{2+}-binding protein NCS1 in liver cancer, we found that high expression of NCS1 and transcriptionally coregulated proteins is associated with an unfavorable clinical outcome in HCC. This study lays the foundation for utilizing NCS1 as a prognostic biomarker in prospective cohorts of HCC patients. Furthermore, our work can serve as a starting point to assess the identified signaling complex and demonstrate a functional contribution to tumorigenesis and metastasis.

Disclosure of Potential Conflicts of Interest

B.E. Ehrlich has ownership interest in and is a consultant/advisory board member for Osmol Therapeutics. No potential conflicts of interest were disclosed by the other authors.

Authors' Contributions

Conception and design: D. Schuette, B.E. Ehrlich
Development of methodology: D. Schuette
Acquisition of data (provided animals, acquired and managed patients, provided facilities, etc.): L.M. Moore
Analysis and interpretation of data (e.g., statistical analysis, biostatistics, computational analysis): D. Schuette, L.M. Moore, B.E. Ehrlich
Writing, review, and/or revision of the manuscript: D. Schuette, M.E. Robert, T.H. Taddei, B.E. Ehrlich
Study supervision: B.E. Ehrlich

Acknowledgments

D. Schuette received a scholarship from the German National Merit Foundation. NIH grant 5P01DK057751 (B.E. Ehrlich and M.E. Robert) supported this work.

Helpful discussions with Michael H. Nathanson (Yale University) and Joseph K. Lim (Yale University) are acknowledged.

The costs of publication of this article were defrayed in part by the payment of page charges. This article must therefore be hereby marked *advertisement* in accordance with 18 U.S.C. Section 1734 solely to indicate this fact.

Received February 7, 2018; revised April 6, 2018; accepted May 17, 2018; published first May 22, 2018.

References

1. Ferlay J, Soerjomataram I, Dikshit R, Eser S, Mathers C, Rebelo M, et al. Cancer incidence and mortality worldwide: sources, methods and major patterns in GLOBOCAN 2012. Int J Cancer 2015;136:E359–86.
2. Ryerson AB, Eheman CR, Altekruse SF, Ward JW, Jemal A, Sherman RL, et al. Annual Report to the Nation on the Status of Cancer, 1975-2012, featuring the increasing incidence of liver cancer. Cancer 2016;122:1312–37.
3. Wong CR, Nguyen MH, Lim JK. Hepatocellular carcinoma in patients with non-alcoholic fatty liver disease. World J Gastroenterol 2016;22: 8294–303.
4. Llovet JM, Ricci S, Mazzaferro V, Hilgard P, Gane E, Blanc J, et al. Sorafenib in advanced hepatocellular carcinoma. N Engl J Med 2008;359:378–90.
5. Berridge MJ. Calcium signalling and cell proliferation. BioEssays 1995;17:491–500.
6. Berridge MJ. Inositol triphosphate and calcium signalling. Nature 1993; 361:315–25.
7. Berridge MJ. Neuronal calcium signaling. Neuron 1998;21:13–26.
8. Chen Y, Chen Y, Chiu W, Shen M. Remodeling of calcium signaling in tumor progression. J Biomed Sci 2013;20:1–10.
9. Prevarskaya N, Skryma R, Shuba Y. Calcium in tumour metastasis: new roles for known actors. Nat Rev Cancer 2011;11:609–18.
10. Moore LM, England A, Ehrlich BE, Rimm DL. Neuronal calcium sensor 1 (NCS-1) promotes tumor aggressiveness and predicts patient survival. Mol Cancer Res 2017;15:942–952.
11. Hass HG, Vogel U, Scheurlen M, Jobst J. Gene-expression analysis identifies specific patterns of dysregulated molecular pathways and genetic subgroups of human hepatocellular carcinoma. Anticancer Res 2016;5096: 5087–95.
12. Wu R, Duan L, Cui F, Cao J, Xiang Y, Tang Y, et al. S100A9 promotes human hepatocellular carcinoma cell growth and invasion through RAGE-mediated ERK1/2 and p38 MAPK pathways. Exp Cell Res 2015;334:228–38.
13. Zhang J, Zhang K, Jiang X. S100A6 as a potential serum prognostic biomarker and therapeutic target in gastric cancer. Dig Dis Sci 2014;59: 2136–44.
14. Luo X, Xie H, Long X, Zhou M, Xu Z, Shi B, et al. EGFRvIII mediates hepatocellular carcinoma cell invasion by promoting S100 calcium binding protein A11 expression. PLoS ONE 2013;8:1–9.
15. Zhang Y, Liu Y, Duan J, Yan H, Zhang J, Zhang H, et al. Hippocalcin-like 1 suppresses hepatocellular carcinoma progression by promoting p21Waf/Cip1stabilization by activating the ERK1/2-MAPK pathway. Hepatology 2016;63:880–97.
16. Koizumi S, Rosa P, Willars GB, Challiss RAJ, Taverna E, Francolini M, et al. Mechanisms underlying the neuronal calcium sensor-1-evoked enhancement of exocytosis in PC12 cells. J Biol Chem 2002;277:30315–24.
17. Weiss JL, Hui H, Burgoyne RD. Neuronal calcium sensor-1 regulation of calcium channels, secretion, and neuronal outgrowth. Cell Mol Neurobiol 2010;:1283–92.
18. Schaad NC, Castrot EDE, Neft S, Hegit S, Hinrichsent R, Martone ME, et al. Direct modulation of calmodulin targets by the neuronal calcium sensor NCS-1. Proc Natl Acad Sci USA 1996;93:9253–8.
19. Choe C, Ehrlich BE. The inositol 1,4,5-trisphosphate receptor (IP3R) and its regulators: sometimes good and sometimes bad teamwork. Sci STKE 2006;2006:re15.
20. Schlecker C, Boehmerle W, Jeromin A, Degray B, Varshney A, Sharma Y, et al. Neuronal calcium sensor-1 enhancement of InsP 3 receptor activity is inhibited by therapeutic levels of lithium. J Clin Invest 2006;116:1–7.
21. Boehmerle W, Splittgerber U, Lazarus MB, McKenzie KM, Johnston DG, Austin DJ, et al. Paclitaxel induces calcium oscillations via an inositol 1,4,5-trisphosphate receptor and neuronal calcium sensor 1-dependent mechanism. Proc Natl Acad Sci USA 2006;103:18356–61.
22. Nakamura TY, Jeromin A, Smith G, Kurushima H, Koga H, Nakabeppu Y, et al. Novel role of neuronal Ca2+ sensor-1 as a survival factor up-regulated in injured neurons. J Cell Biol 2006;172:1081–91.
23. Gromada J, Bark C, Smidt K, Efanov AM, Janson J, Mandic SA, et al. Neuronal calcium sensor-1 potentiates glucose-dependent exocytosis in pancreatic islet cells through activation of phosphatidylinositol 4-kinase beta. Proc Natl Acad Sci USA 2005;102:10303–8.
24. Blasiole B, Kabbani N, Boehmler W, Thisse B, Thisse C, Canfield V, et al. Neuronal calcium sensor-1 gene ncs-1a is essential for semicircular canal formation in zebrafish inner ear. J Neurobiol 2005;64:285–97.
25. Zhang K, Heidrich FM, Degray B, Boehmerle W, Ehrlich BE. Paclitaxel accelerates spontaneous calcium oscillations in cardiomyocytes by interacting with NCS-1 and the InsP 3 R. J Mol Cell Cardiol 2010;49: 829–35.
26. Weiss JL, Archer DA, Burgoyne RD. Neuronal Ca sensor-1/frequenin functions in an autocrine pathway regulating Ca channels in bovine adrenal chromaffin cells. J Biol Chem 2000;275:40082–7.
27. R Team. R: A language and environment for statistical computing; 2017. Available from: https://www.r-project.org/.
28. The Cancer Genome Atlas Network. Comprehensive and integrative genomic characterization of hepatocellular carcinoma. Cell 2017;169:1327–41.
29. The Cancer Genome Atlas Network. Comprehensive genomic characterization of squamous cell lung cancers. Nature 2012;489:519–25.
30. The Cancer Genome Atlas Network. Comprehensive molecular portraits of human breast tumours. Nature 2012;490:61–70.
31. The Cancer Genome Atlas Network. Comprehensive molecular profiling of lung adenocarcinoma. Nature 2014;511:543–50.
32. Kassambara ANT, Kosinski M. survminer: Drawing Survival Curves using 'ggplot2'. 2017.
33. Benjamin DJ, Berger JO, Johannesson M, Nosek BA, Wagenmakers E, Berk R, et al. Redefine statistical significance. Nat Hum Behav 2017;2:6–10.
34. Paquette J, Tokuyasu T. EGAN: exploratory gene association networks. Bioinformatics 2010;26:285–6.
35. Chaisaingmongkol J, Budhu A, Dang H, Ruchirawat M, Wang XW. Common molecular subtypes among asian hepatocellular carcinoma and cholangiocarcinoma. Cancer Cell 2017;32:57–70.
36. Fujimoto A, Furuta M, Totoki Y, Tsunoda T, Kato M, Shiraishi Y, et al. Whole-genome mutational landscape and characterization of noncoding and structural mutations in liver cancer. Nat Genet 2016;48:500–9.
37. Saha A, Kim Y, Gewirtz ADH, Jo B, Gao C, Ian C, et al. Co-expression networks reveal the tissue-specific regulation of transcription and splicing. Genome Res 2017;27:1–16.
38. Kutsenko A, Ladenheim MR, Kim N, Nguyen P, Chen V, Jayasekera C, et al. Increased prevalence of metabolic risk factors in Asian Americans with hepatocellular carcinoma. J Clin Gastroenterol 2017;51:384–90.

39. Bibonne A, Néant I, Batut J, Leclerc C, Moreau M, Gilbert T. Three calcium-sensitive genes, fus, brd3 and wdr5, are highly expressed in neural and renal territories during amphibian development. Biochim Biophys Acta 2013; 1833:1665–71.
40. Rahl PB, Lin CY, Seila AC, Flynn RA, Mccuine S, Burge CB, et al. c-Myc regulates transcriptional pause release. Cell 2010;141:432–45.
41. Karatas H, Li Y, Liu L, Ji J, Lee S, Chen Y, et al. Discovery of a highly potent, cell-permeable macrocyclic peptidomimetic (MM-589) targeting the WD repeat domain 5 protein (WDR5)–mixed lineage leukemia (MLL) protein–protein interaction. J Med Chem 2017;60:4818–39.
42. Schapira M, Tyers M, Torrent M, Arrowsmith CH. WD40 repeat domain proteins: a novel target class? Nat Rev Drug Discov 2017;16: 773–86.
43. Thomas LR, Wang Q, Grieb BC, Phan J, Foshage AM, Olejniczak ET, et al. Interaction with WDR5 promotes target gene recognition and tumorigenesis by MYC. Mol Cell 2015;58:440–52.
44. Quagliata L, Matter MS, Piscuoglio S, Arabi L, Ruiz C, Procino A, et al. Long noncoding RNA HOTTIP/HOXA13 expression is associated with disease progression and predicts outcome in hepatocellular carcinoma patients. Hepatology 2014;59:911–23.
45. Dong H, Zhang L, Qian Z, Zhu X, Zhu G, Chen Y. Identification of HBV-MLL4 integration and its molecular basis in Chinese hepatocellular carcinoma. PLoS One 2015;10:e0123175.
46. Olson MF, Sahai E. The actin cytoskeleton in cancer cell motility. Clin Exp Metastasis 2009;26:273–87.
47. Li R, Doherty J, Antonipillai J, Chen S, Devlin M, Visser K, et al. LIM kinase inhibition reduces breast cancer growth and invasiveness but systemic inhibition does not reduce metastasis in mice. Clin Exp Metastasis 2013;30:483–95.
48. Takemura M, Mishima T, Wang Y, Kasahara J, Fukunaga K, Ohashi K, et al. Ca 2+/calmodulin-dependent protein kinase IV-mediated LIM kinase activation is critical for calcium signal-induced neurite outgrowth. J Biol Chem 2009;284:28554–62.
49. Aoki T, Ueda S, Kataoka T, Satoh T. Regulation of mitotic spindle formation by the RhoA guanine nucleotide exchange factor ARHGEF10. BMC Cell Biol 2009;10:1–16.
50. Hanna S, El-Sibai M. Signaling networks of Rho GTPases in cell motility. Cell Signal 2013;25:1955–61.
51. Prunier C, Prudent R, Kapur R, Sadoul K. LIM kinases: cofilin and beyond. Oncotarget 2017;8:41749–63.
52. Nakagawa S, Wei L, Song WM, Zhang B, Fuchs BC, Hoshida Y. Liver cancer prevention in cirrhosis by organ transcriptome analysis and lysophosphatidic acid pathway inhibition. Cancer Cell 2016;30:879–90.
53. Aran D, Camarda R, Odegaard J, Paik H, Oskotsky B, Krings G, et al. Comprehensive analysis of normal adjacent to tumor transcriptomes. Nat Commun 2017;8:1–13.

THE FASEB JOURNAL • RESEARCH • www.fasebj.org

Neuronal calcium sensor 1 (NCS1) promotes motility and metastatic spread of breast cancer cells *in vitro* and *in vivo*

Jonathan E. Apasu,[*,1] Daniel Schuette,[*] Ryan LaRanger,[†] Julia A. Steinle,[*,2] Lien D. Nguyen,[*] Henrike K. Grosshans,[*] Meiling Zhang,[‡] Wesley L. Cai,[‡] Qin Yan,[‡] Marie E. Robert,[‡] Michael Mak,[†] and Barbara E. Ehrlich[*,3]

[*]Department of Pharmacology, [†]Department of Biomedical Engineering, and [‡]Department of Pathology, Yale University, New Haven, Connecticut, USA

ABSTRACT: Increased levels of the calcium-binding protein neuronal calcium sensor 1 (NCS1) predict an unfavorable patient outcome in several aggressive cancers, including breast and liver tumors. Previous studies suggest that NCS1 overexpression facilitates metastatic spread of these cancers. To investigate this hypothesis, we explored the effects of NCS1 overexpression on cell proliferation, survival, and migration patterns *in vitro* in 2- and 3-dimensional (2/3-D). Furthermore, we translated our results into an *in vivo* mouse xenograft model. Cell-based proliferation assays were used to demonstrate the effects of overexpression of NCS1 on growth rates. *In vitro* colony formation and wound healing experiments were performed and 3-D migration dynamics were studied using collagen gels. Nude mice were injected with breast cancer cells to monitor NCS1-dependent metastasis formation over time. We observed that increased NCS1 levels do not change cellular growth rates, but do significantly increase 2- and 3-D migration dynamics *in vitro*. Likewise, NCS1-overexpressing cells have an increased capacity to form distant metastases and demonstrate better survival and less necrosis *in vivo*. We found that NCS1 preferentially localizes to the leading edge of cells and overexpression increases the motility of cancer cells. Furthermore, this phenotype is correlated with an increased number of metastases in a xenograft model. These results lay the foundation for exploring the relevance of an NCS1-mediated pathway as a metastatic biomarker and as a target for pharmacologic interventions.—Apasu, J. E., Schuette, D., LaRanger, R., Steinle, J. A., Nguyen, L. D., Grosshans, H. K., Zhang, M., Cai, W. L., Yan, Q., Robert, M. E., Mak, M., Ehrlich, B. E. Neuronal calcium sensor 1 (NCS1) promotes motility and metastatic spread of breast cancer cells *in vitro* and *in vivo*. FASEB J. 33, 4802–4813 (2019). www.fasebj.org

KEY WORDS: cell migration · xenograft model · calcium binding protein · metastasis · Ca^{2+} signaling

A hallmark of aggressive tumors is their ability to invade tissues and metastasize to distant organs (1). It is well known that the majority of tumor-related deaths are attributable to dissemination of cancer cells throughout the body (2, 3). Nevertheless, many of the mechanisms that favor the spread of tumor cells to distant sites in the body remain to be elucidated (1, 4).

Calcium (Ca^{2+}) is a crucial second messenger molecule. It enters the cytoplasm *via* voltage- or ligand-gated channels (5, 6) from 2 major sources, the extracellular space and intracellular Ca^{2+} storage compartments such as the endoplasmic reticulum (7) and the mitochondria (8). Release of Ca^{2+} from intracellular compartments often follows oscillatory patterns, which can lead to reprogramming of the transcriptional machinery of mammalian cells (9–11). Alterations in cytoplasmic Ca^{2+} regulate critical cellular processes such as proliferation, cell growth, cell cycle progression (12), neurogenesis (6, 13, 14), and apoptotic cell death (12, 15).

The coordinated movement of cells largely depends on tightly regulated spatiotemporal Ca^{2+} signals (16–20). Given these properties of the physiologic function of Ca^{2+}, dysregulated Ca^{2+} pathways were recently recognized to be possible drivers of aggressive, highly metastatic cancers (21–24). A variety of proteins that are involved in regulating and amplifying Ca^{2+} signals in mammalian cells have been implicated in cancer progression, including

ABBREVIATIONS: 2/3-D, 2-dimensional; GFP, green fluorescent protein; H&E, hematoxylin and eosin; HEK-293, human embryonic kidney 293; IHC, immunohistochemistry; InsP3R, inositol 1,4,5-*tris*phosphate receptor; MSD, mean squared displacement; NCS1, neuronal calcium sensor 1; NCS1-OE, NCS1-overexpressing; PI4K, phosphatidylinositol 4-OH kinase

[1] Current affiliation: University of Bonn, Bonn, Germany.
[2] Current affiliation: University of Muenster, Muenster, Germany.
[3] Correspondence: Department of Pharmacology, Yale University, 333 Cedar St., Room B-147, P.O. Box 208026, New Haven, CT 06520-8066, USA. E-mail: barbara.ehrlich@yale.edu

doi: 10.1096/fj.201802004R
This article includes supplemental data. Please visit *http://www.fasebj.org* to obtain this information.

0892-6638/19/0033-4802 © FASEB

S100 Ca^{2+}-binding proteins (25) and visinin-like protein 1 (VILIP1) (26). The fact that cell motility is regulated by Ca^{2+} as a second messenger suggests that molecules which bind Ca^{2+} and mediate its downstream effects could be potential cancer biomarkers as well as therapeutic targets.

One example of a Ca^{2+} regulated kinase involved in cell movement is LIM domain kinase 1 (LIMK1) (16). LIMK1 regulates the organization of the actin cytoskeleton *via* phosphorylation of its downstream effector cofilin (27). Cancer cells rely on increased levels of LIMK1 to be able to invade the tissue that surrounds the tumor (28) and inhibition of LIMK1 reduces their invasiveness (29, 30).

Neuronal calcium sensor 1 (NCS1) is a ubiquitously expressed Ca^{2+} binding protein (31, 32) with the highest levels of expression being found in the CNS (33). It is closely related to other members of the NCS family of proteins (34) such as hippocalcin or recoverin. On the structural level, NCS proteins are composed of 4 EF-hand domains that are canonical Ca^{2+} binding sites and a myristoylation site at the N terminus (31). NCS1 interacts with a wide range of proteins, including the inositol 1,4,5-*tris*phosphate receptor (InsP3R), dopamine receptor type 2 (D2R), and phosphatidylinositol 4-OH kinase (PI4K) (35, 36). Through its protein–protein interactions, NCS1 regulates vital cellular processes such as neurotransmitter release (32), neurite outgrowth and neuronal survival (37, 38), spatial memory formation (31), and the InsP3R signaling pathway (39, 40).

We have previously described NCS1 as a prognostic biomarker in cohorts of breast (41) and liver (42) cancer patients and demonstrated that the overexpression of NCS1 leads to a marked increase in invasion and motility *in vitro* (41) using 2-dimensional (2-D) assays. Furthermore, NCS1 expression levels are highly correlated with other components of Ca^{2+} signaling as well as LIMK1 expression (42). In this study, we investigated the hypothesis that increased expression of NCS1 facilitates the formation of distant metastases by enhancing cellular motility. *In vitro* cell culture models of NCS1 overexpression were used to demonstrate that NCS1 levels do not modulate proliferation rates but do modulate cell motility in 2- and 3-D environments. We validated these results in a mouse model, showing that NCS1 facilitates early metastatic spread of tumor cells and increases the survival of cancer cells in more mature tumors.

MATERIALS AND METHODS

Cell culturing

MDA-MB-231 cells were obtained from the American Type Culture Collection (ATCC; Manassas, VA, USA). ATCC validates all cell lines by Short Tandem Repeat Analysis. The MDA-MB-231 cells were transduced with a NCS1 overexpression vector and a control vector as previously described (41). The MDA-MB-231 cell lines were maintained at 37°C, 5% CO_2 in DMEM medium supplemented with 10% fetal bovine serum, 1% L-glutamine and 1% penicillin/streptomycin.

Cell proliferation assays

For the CellTiter-Glo assay, 1000 cells/well were plated into sterile 96-well plates and grown over a period of 5 d. The relative number of viable cells was determined every day for 10 wells of such a plate using CellTiter-Glo reagent (Promega, Madison, WI, USA) and a microplate reader (Tecan Infinite M1000 Pro; Tecan Trading, Männedorf, Switzerland) according to the manufacturers' instructions. Every well was used just once and the marginal wells were never used. Three independent experiments were performed using NCS1-overexpressing (OE) MDA-MB-231 cells and control cells, and all measurements were normalized to the average luminescence on d 1.

For the AlamarBlue assay, 8 replicates of 1250, 2500, 5000, and 10,000 cells/well were plated into sterile 96-well plates. After a 24-h incubation period, medium was removed and 100 μl fresh medium with an additional 10 μl AlamarBlue reagent (Thermo Fisher Scientific, Waltham, MA, USA) was added to each well. After another 2 h of incubation, a fluorescence signal was measured using the aforementioned microplate reader.

Scratch assay and colony formation assay

Scratch assays were performed as previously described (41). Cells were serum starved 12 h prior to the experiment to inhibit cell proliferation. For quantification, ImageJ (National Institutes of Health, Bethesda, MD, USA) was used and the distance traveled was calculated after 24 h. The mean distance traveled was plotted for $n = 3$ independent experiments.

For colony formation assays, cells were cultured per standard protocol in T75 flasks. Once cell confluence approached 80–90%, the cells were detached by the addition of 2 ml TrypLE (Thermo Fisher Scientific, Rockford, IL, USA), followed by dilution in 5 ml of fresh medium. Cell concentration was determined using a hematocytometer. Subsequently, a total number of 100, 200 or 500 cells was added to each well of a 12-well plate. Cells were then left undisturbed in the incubator for 14 d. After 14 d, colonies were fixed and stained with 2.5% crystal violet solution and were subsequently washed to remove excess dye and scanned with a conventional scanner. The total area covered was determined with ImageJ (43). Data were obtained from 3 independent experiments with 4 replicates in each experiment. Data were represented as total area covered in each individual well.

Quantitative RT-PCR

RNA was isolated using the RNeasy Mini Kit (Qiagen, Hilden, Germany) according to the manufacturer's instructions. Using a High-Capacity cDNA Reverse Transcription Kit (4368814; Thermo Fisher Scientific) according to the manufacturer's protocol, 0.5–1 μg of RNA was then transcribed to cDNA. Quantitative real-time PCR was performed using Power SYBR Green Master Mix reagent and a 7300 Real-Time PCR System (Thermo Fisher Scientific). The $\Delta\Delta C_t$ method (44) was used to calculate expression fold changes with ACTB (β-actin) and ribosomal protein S18 as control genes. The following primers were used at a concentration of 5 μM: NCS1 (forward, 5′-GATGCTGGACATTGTGGATG-3′; reverse, 5′-CTTGGAACCCTCCTGGAACT-3′), ACTB (forward, 5′-GTCTTCCCCTCCATCGTGG-3′; reverse, 5′-GATGCCTCTCTTGCTCTGGG-3′), and S18 (forward, 5′-TTCGAACGTCTGCCCTATCAA-3′; reverse, 5′-ATGGTAGGCACGGCGACTA-3′).

Assessment of NCS1 protein levels

MDA-MB-231 cells were lysed in ice-cold M-PER Mammalian Protein Extraction Reagent buffer (Thermo Fisher Scientific) supplemented with a protease inhibitor. Protein concentrations were determined using the Bio-Rad protein assay reagent (San Diego, CA, USA). SDS-PAGE was performed with 30 μg of protein. Briefly, the protein was transferred to a nitrocellulose membrane (GE Healthcare, Chicago, IL, USA), the resulting blots were blocked for 1 h in 5% nonfat dry milk in Tris-buffered saline with 0.1% Tween 20 (TBST), and were then incubated with a primary NCS1-specific antibody (sc-13037, diluted 1:5000; Santa Cruz Biotechnology, Dallas, TX, USA) or β-actin–specific antibody (sc-47778, diluted 1:1000; Santa Cruz Biotechnology) over night at 4°C. All dilutions are vol/vol. Blots were then incubated with horseradish peroxidase and labeled goat anti-rabbit IgG (diluted 1:10,000; Santa Cruz Biotechnology) at room temperature for 1 h. Ultimately, protein bands were visualized using electrochemiluminescence detection reagents (Thermo Fisher Scientific).

Immunofluorescence microscopy

Control and NCS1-OE cells were seeded on sterile 22 × 22-mm glass coverslips at a density of 50,000 cells/coverslip. Medium was removed 24 h after seeding, and each coverslip was briefly washed twice with 2 ml of 1× PBS (pH 7.4; AmericanBio, Natick, MA, USA) each time. Fixation was performed for 15 min at room temperature with a 4% paraformaldehyde solution (pH 7.4). Following 3 washes with 2 ml PBS, cells were permeabilized and blocked in PBS solution containing 1% bovine serum albumin (0.1% Triton-X 100; AmericanBio) for 1 h at room temperature. Following blocking, cells were incubated with a rabbit anti-NCS1 pAb diluted in blocking solution (sc-13037, diluted 1:100; Santa Cruz Biotechnology) overnight at 4°C. After extensive washing with PBS, cells were incubated with an AlexaFluor-488 goat anti-rabbit secondary antibody (diluted 1:1000; Thermo Fisher Scientific) and a rhodamine-conjugated phalloidin (diluted 1:1000 dilution; Thermo Fisher Scientific) for 2 h at room temperature in the dark. Cells were then washed extensively with PBS before being mounted on glass slides with antifade medium ProLong Gold with DAPI (Thermo Fisher Scientific). Slides were cured overnight before images were captured with a confocal microscope using the ×100 lens (LSM 710 Duo; Carl Zeiss, Oberkochen, Germany). A laser power of 0.5% was used to detect NCS1 in overexpressing cells and 10% to detect NCS1 in control cells. All other settings were kept the same among all coverslips.

Transduction of cells with a reporter for bioluminescent imaging

Previously (41) generated NCS1-OE and control MDA-MB-231 cells were retro-virally infected with a triple-fusion protein reporter. The reporter encodes for herpes simplex virus thymidine kinase 1, green fluorescent protein (GFP) and firefly luciferase (45). Human embryonic kidney 293 (HEK-293) cells were used to produce viruses. They were transduced using the Clontech Calcium Phosphate Transfection Kit (Clontech Laboratories, Mountain View, CA, USA) and a polybrene-facilitated infection of MDA-MB-231 cells. Briefly, HEK-293 cells were plated on a 10 cm dish 1 d before the transfection for producing retrovirus and grown to 60% confluence. The next day, 20 μg of retroviral vector DNA and packaging plasmids [envelope, vesicular stomatitis virus (VSVG) 6 μg; 10μg pMDLg/pRRE 3rd generation lentiviral packaging plasmid containing Gag and Pol, 5μg pRSV-Rev 3rd generation lentiviral packaging plasmid containing Rev (or HIV1gp6)] were mixed with 4-(2-hydroxyethyl)-1-piperazineethanesulfonic acid–buffered saline to obtain a 1-time solution and were then incubated for 15 min. Then, the plasmid-containing solution was added drop-wise to the HEK-293 cells and fresh medium was applied after 6 h. The HEK-293 cells were examined for GFP positivity 2 d after transfection by using a microscope to measure green fluorescence. The retrovirus-containing supernatant was collected on d 2 and 3 after transfection and was centrifuged and filtered using a 0.45-μm filter.

MDA-MB-231 cells were incubated with the virus-containing solution and 4 μg/ml polybrene for 6 h. The medium was changed after the 6 h incubation and later on d 4. On d 6, the MDA-MB-231 cells were checked for GFP expression. The MDA-MB-231 cells were harvested 48 h posttransduction in ice-cold PBS and were passed through a 70-μM filter. After 2 washing cycles, cells were prepared in PBS at a concentration of 5–10 million/ml. Cells were sorted for GFP positivity using a FACSAria-B high-speed cell sorter (BD Biosciences, San Jose, CA, USA). GFP positive cells were collected and transferred to a sterile plastic flask for further culturing.

Assessment of bioluminescence

The Promega Luciferase Assay System was used to quantify bioluminescence. Cells were prepared in a 96-well plate according to the manufacturer's instructions. Luciferin was added to the wells 20 s before measuring luminescence using a Tecan Infinite M1000 Pro microplate reader.

Cell migration assay

Embedding MDA-MB-231 cancer cells in a 3-D collagen I matrix

Engineered MDA-MB-231 cells were suspended at a concentration of 10 million cells/ml in tissue culture media. A collagen gel was made by adding a calculated amount of 0.5 N NaOH to neutralize a mixture of double-distilled H_2O and acetic acid–solubilized type I rat tail collagen (Corning, Corning, NY, USA) on ice for a final collagen concentration of 4 mg/ml. Suspended cells were then added to the gel at a 1:10 dilution for a final cell concentration of 1×10^6 cells/ml. The gels were then transferred to a 24-well glass-bottomed cell culture plate (MatTek, Ashland, MA, USA) kept on an ice pack. Once all gels were transferred to the 24-well plate, the plate was transferred to an incubator at 37°C with 5% CO_2. The sample was flipped several times during gelation to prevent cell sediment from forming on the bottom of the plate. After 1 h, tissue culture media was added to the gels, which were subsequently maintained at 37°C with 5% CO_2.

Analysis of cell shape, velocity, and mean squared displacement

A Leica SP8 confocal microscope (Wetzlar, Germany) using a ×20 objective was used to image the cells. A temperature of 37°C and a 5% CO_2 atmosphere were maintained using a humidified OKO labs live cell imaging incubator. For each well, 250 μm z stacks were created using 10 slices ≥50 μm from the bottom of the well. Images were taken every 5 min for 8 h to create the final hyperstacks. The perimeter, circularity, and aspect ratio of the cells were measured by tracing the edges of z projections of 20 cells using ImageJ. Cell migration was tracked by first taking a z projection of the hyperstack to create a 2-D representation of 3-D migration of the cells. Cell migration was then manually tracked using the point selection tool in ImageJ across 8 h of hyperstack data. The resulting output was analyzed using custom scripts in MatLab (MathWorks, Natick, MA, USA). The average speed of

each condition was determined by measuring the average speed of each cell at each time step, and then averaging this average cell speed for 40 cells across all conditions. The mean squared displacement (MSD) was calculated as

$$\mathrm{MSD}(\Delta t) = < [x(t+\Delta t) - x(t)]^2 + [y(t+\Delta t) - y(t)]^2 >$$

where Δt is time interval, $x(t)$ and $y(t)$ are spatial coordinates at time t, and $< \ldots >$ indicates the average over all available starting times. An average of the MSDs at the longest interval (8 h) was calculated for 40 cells per condition. Static trajectories and graphs of MSDs were also created using custom scripts in MatLab.

Animal studies: tail vein injection

All mouse work was done in accordance with the Yale University Institutional Animal Care and Use Committee. Female athymic nude mice (7–9 wk old) were obtained from Envigo (Somerset, NJ, USA) for the xenografting study. For each mouse, 4×10^5 MDA-MB-231 cells were harvested, washed in PBS, resuspended in 0.1 ml sterile saline, and injected into the lateral tail vein. The mice were imaged directly after the tail vein injection and unsuccessfully xenografted mice were excluded from the study.

Mouse imaging studies, data analysis, and lung harvest

After anesthetizing mice by intraperitoneal injection of 0.2 ml 10% ketamine/1% xylazine in sterile saline, they were retro-orbitally injected with 0.1 ml luciferin. The mice were imaged within 2–5 min of the retro-orbital injection using a Perkin-Elmer Ivis system coupled with Live Image acquisition and analysis software. The photon flux from the xenografted cells in the lungs of each mouse was evaluated by selecting a rectangular region of interest over the lung. All obtained values were normalized to the photon flux obtained immediately after xenografting, resulting in an initial bioluminescence signal of 1 for every mouse.

Lungs for histopathologic evaluation were harvested on d 3 and 7 and at the end of the study. The lungs were harvested after the aforementioned *in vivo* imaging of xenografted mice and after perfusion with 10 ml ice-cold Dulbecco's PBS. The harvested lungs were washed in ice-cold Dulbecco's PBS and imaged with Ivis to obtain an *ex-vivo* lung bioluminescence signal.

Histopathologic assessment of lung specimens

Harvested lung tissue was placed in 10% formalin for fixation. After fixation, the lungs were paraffin embedded and hematoxylin and eosin (H&E)–stained slides were generated by Yale Mouse Pathology. Anti-NCS1 immunohistochemical staining using a previously described antibody (41) was performed by Yale Research Histology to confirm the presence of human NCS1-positive MDA-MB-231 cells in the xenografted lungs. All slides underwent blind evaluation by an experienced pathologist.

Statistical analysis

Unless noted otherwise, all analyses were done using the Python programming language (v.3.6; *https://www.python.org/*). An independent 2-sample Student's t test was used to compare the mean values of 2 independent datasets; values of $P < 0.05$ were considered significant. Whenever possible, error bars were plotted indicating either 95% confidence intervals or the means ± SEM.

RESULTS

Overexpression of NCS1 changes the cellular phenotype without affecting proliferation rates

To explore the *in vitro* function of NCS1 in malignant tumors, we stably overexpressed NCS1 in MDA-MB-231 breast cancer cells (referred to as NCS1-OE) using a previously described protocol (41). Immunoblotting was performed to confirm successful overexpression of the target gene (**Fig. 1*A***). Real-time quantitative PCR measurements confirmed that NCS1 mRNA expression levels were, on average, 4-fold higher in NCS1-OE cells than in the controls. This result was consistent when normalized to 2 different housekeeping genes ($P < 0.01$, Supplemental Fig. S1).

To determine whether NCS1 overexpression enhances the aggressiveness of tumor cells by increasing their proliferation rates, cell growth of NCS1-OE and control cells was measured over a period of 5 d (Fig. 1*B*) using an ATP-based growth assay. As expected from previously reported results (41), no differences in proliferation rates were observed. To validate this result, we performed an AlamarBlue assay (Supplemental Fig. S2). Again, proliferation rates of NCS1-OE and control cells were similar. During the course of these experiments it became clear that the overexpression of NCS1 led to a marked change in cellular morphology in a 3-D environment (Fig. 1*C*). Specifically, NCS1-OE cells were significantly less rounded with a higher aspect ratio than the control (**$P < 0.01$, ***$P < 0.001$, Fig. 1*D*). Furthermore, NCS1-OE cells had a significantly higher cell perimeter (Supplemental Fig. S3). Large cellular protrusions were seen exclusively in the NCS1-OE context (Supplemental Fig. S4), suggesting that this newly acquired phenotype predicts the functional consequences of cellular motility, metastatic behavior, and survival (46, 47).

Immunofluorescence microscopy shows that NCS1 preferentially localizes to cell protrusions in control and NCS1-OE cells

To further investigate the localization of NCS1 in control and NCS1-OE MDA-MB231 cells, immunofluorescence imaging was performed (**Fig. 2*A*, *B***). As a result, NCS1 was found to be localized at cellular protrusions, including the lamellopodia. NCS1 also colocalizes extensively with actin at the leading edge, but not with cytoplasmic actin puncta or stress fibers.

NCS1 overexpression increases colony formation and cell motility in 2- and 3-D *in vitro* assays

To further investigate the hypothesis that NCS1 favors tumor growth and metastatic spread through increasing survival and motility instead of proliferation, a colony formation assay was performed. Different numbers of cells were plated in a cell culture dish and grown for 14 d. After

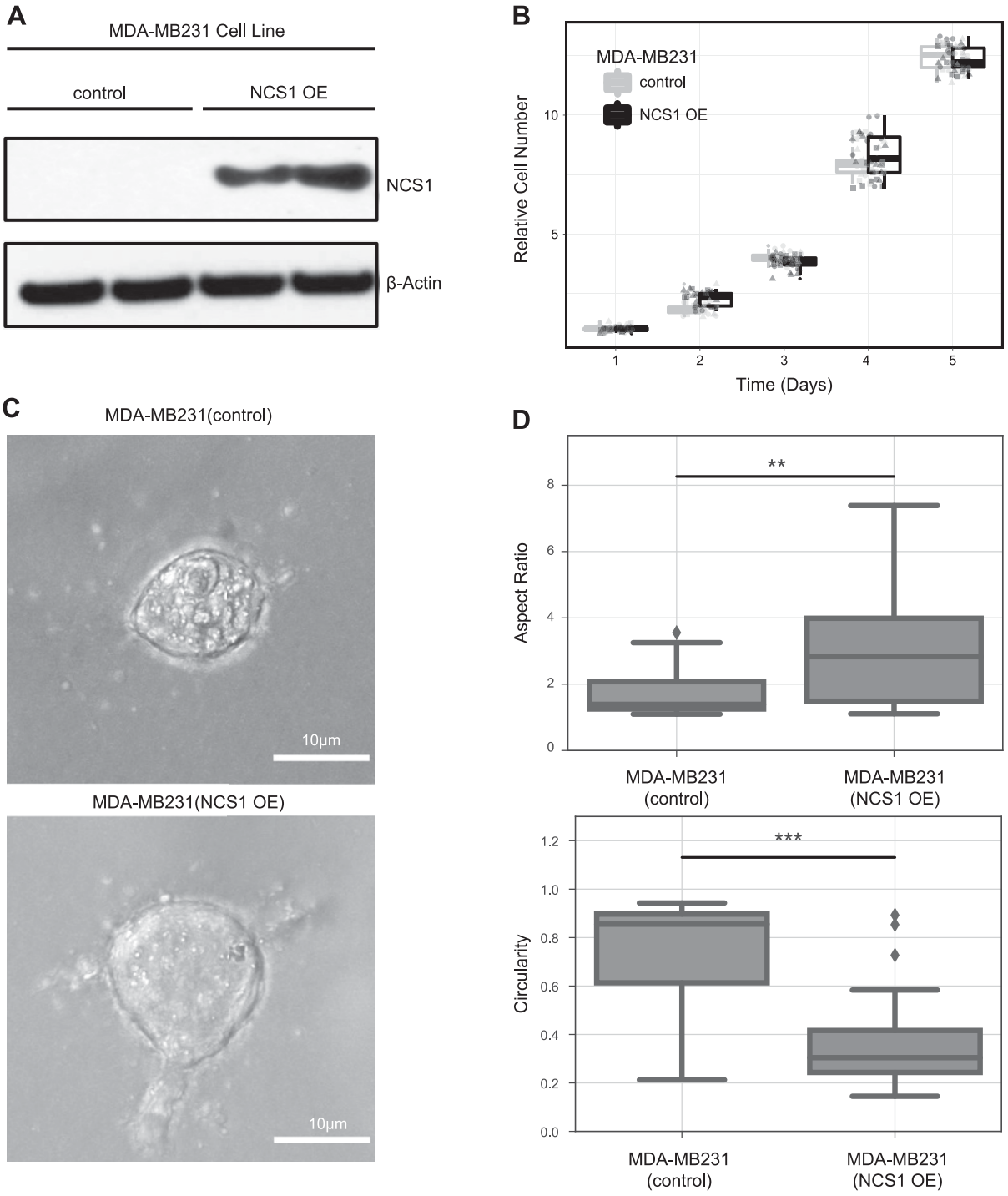

Figure 1. NCS1 overexpression changes cellular morphology of MDA-MB231 cells without affecting proliferation rates. *A*) Immunoblot showing control and NCS1-OE MDA-MB231 cells. Actin is used as a loading control. Longer exposure shows NCS1 expression in control cells, as previously demonstrated (41). *B*) Box plots demonstrating proliferation rates of MDA-MB231 control and NCS1-OE cells continuously over 5 d. Circles, triangles, and squares represent different biologic replicates. An ATP dye was used to measure the absolute cell number and all values were normalized to the mean on d 0 before plotting. *C*) Brightfield microscopy images of single MDA-MB231 control and NCS1-OE cells showing the different morphologies of these genotypes. Cells were grown in 3-D collagen gels identical to the gels used for subsequent experiments (*e.g.*, Fig. 3*C–E*). *D*) Box plots showing the aspect ratio and circularity of MDA-MB231 control and NCS1-OE cells ($n = 20$). $^{**}P < 0.01$, $^{***}P < 0.001$.

fixing and staining the resulting colonies, the total area covered by cells was calculated. Compared with the control, the NCS1-OE cells showed a significantly increased ability to form colonies ($P < 0.01$; **Fig. 3*A***). These differences were consistently found with different starting cell numbers (Fig. 3*A*). Thus, high NCS1 expression increases the capacity of cancer cells to form colonies *in vitro*, which mimics a metastatic setting.

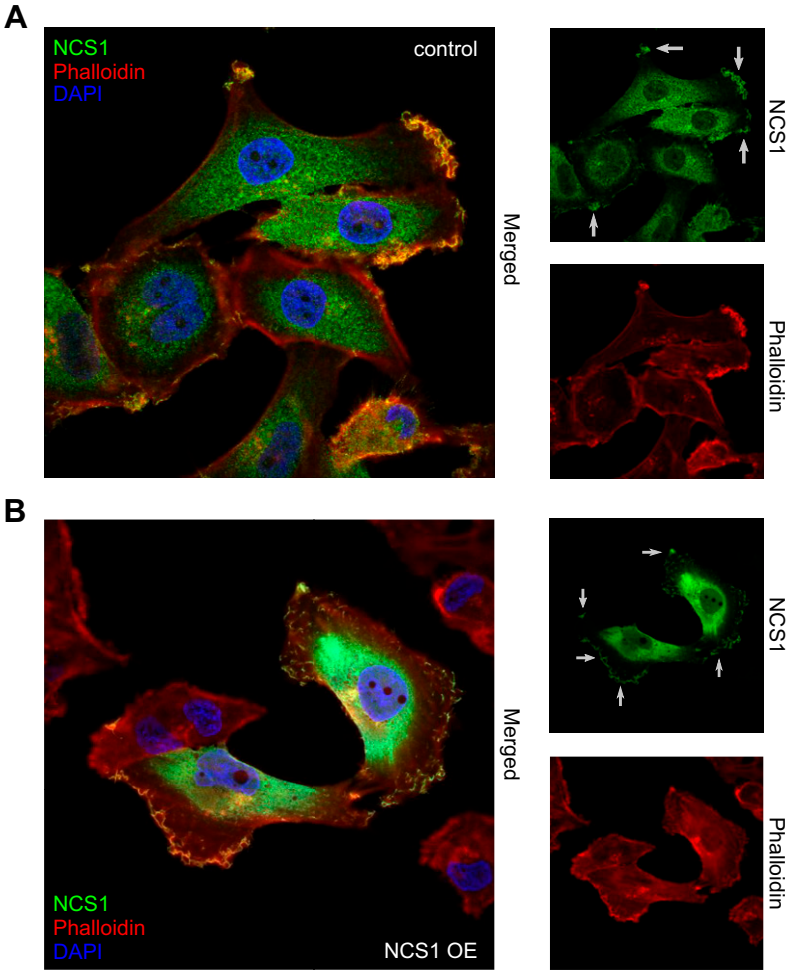

Figure 2. NCS1 localizes to the leading edge of MDA-MB231 control and NCS1-OE cells. *A*) Immunofluorescence microscopy image of control MDA-MB231 cells. The large panel shows a merged image of DAPI (blue), phalloidin (to stain for actin; red), and anti-NCS1 (green) stainings. The smaller panels show the same anti-NCS1 and Phalloidin stainings but separately. Small gray arrows point at localized NCS1. *B*) Immunofluorescence microscopy image of NCS1-OE MDA-MB231 cells. The large panel shows a merged image of DAPI (blue), Phalloidin (red), and anti-NCS1 (green) stainings. The smaller panels show the same anti-NCS1 and Phalloidin stainings but separately. Small gray arrows point at localized NCS1. Note that the laser power used to image the control cells in *A* was the original magnification and is ×20 larger than the NCS1-OE cells in *B*.

To monitor *in vitro* 2-D motility, assay cells were placed in a cell culture dish and a standardized wound was applied to the cell monolayer. Then, wound closure was quantified using the relative distance that control and NCS1-OE cells had traveled after 24 h. NCS1-OE cells closed the scratched area in the monolayer significantly ($P < 0.01$) more than the control cells, indicating an enhanced 2-D migration of NCS1-OE cells (Fig. 3*B*).

Next, a 3-D migration assay was performed to validate these findings. NCS1-OE and control MDA-MB231 cells were placed in a collagen matrix and time-lapse microscopy was performed to capture the movement of many cells simultaneously over time. The overall trajectory of 20 cells per condition is shown in Fig. 3*C*, where each colored trace is a single cell that was tracked over time, demonstrating that there was considerably more movement in the NCS1-OE condition. This movement did not have a directional bias. NCS1-OE cells showed increased MSD after 8 h, indicating that the NCS1-OE cells experienced significantly more net displacement ($P < 0.005$; Fig. 3*D*). Also, the average cell velocity in the NCS1-OE cells was significantly higher than in the control cells ($P < 0.001$; Fig. 3*E*). These results show that the NCS1-OE cells are better able to migrate through a 3-D collagen gel, which indicates that these cells would be more prone to metastatic migration *in vivo*.

NCS1-OE cells exhibit an increased capacity to metastasize *in vivo*

Given these changes in cellular phenotype, colony formation, and migratory capacity that are induced by overexpression of NCS1, we next studied NCS1 in an *in vivo* setting. Female nude mice were injected with MDA-MB231 cells that were engineered to express a firefly luciferase reporter and either NCS1 ($NCS1^+$) or an empty vector (control). Photon flux was utilized as a metric of relative tumor amount in the mouse lungs. The total flux was calculated from lung imaging studies on d 0, 1, 3, 7, 14, 21, and 28 (**Fig. 4*A***) after tail vein injection with the respective tumor cells. The majority of cells were observed in the lungs. No luminescence signal was found in other organs (Supplemental Fig. S5). All measurements were normalized to the total flux on d 0 to permit comparisons among individual mice. Figure 4*B* shows representative results for 2 mice and Fig. 3*C* shows the relative flux for all mice (see Supplemental Fig. S6 for a validation experiment with a longer follow-up).

Whereas the growth rates of $NCS1^+$ and control tumors are comparable from d 7 onwards, the biggest difference between the groups can be observed between d 0 and 7. Consistent with our *in vitro* results, these *in vivo* findings suggest that NCS1-OE tumor cells have a survival advantage in the early phase of tumor development (Fig. 4*C*).

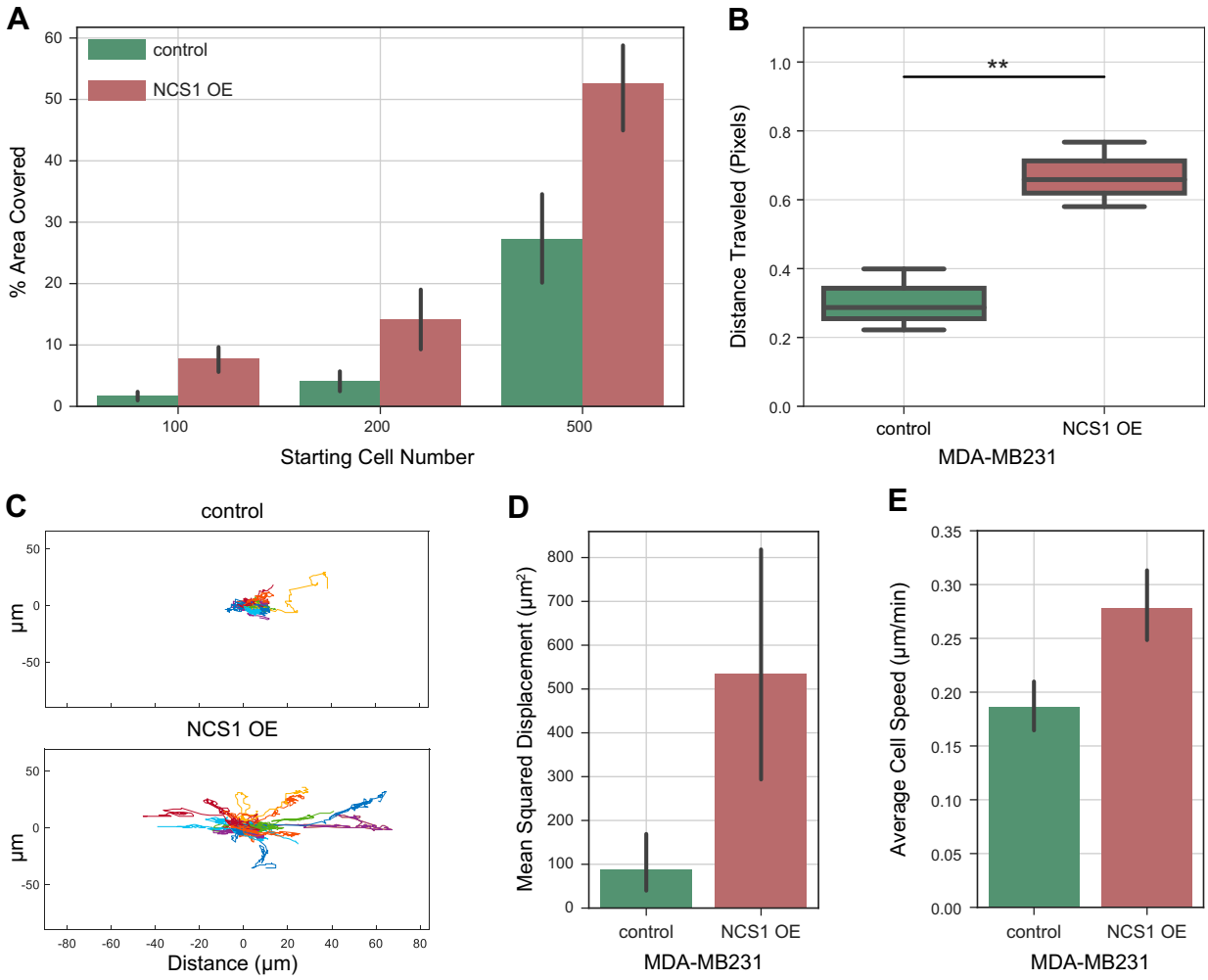

Figure 3. NCS1 overexpression increases cellular motility in 2- and 3-D cell culture experiments. *A*) Bar plot of a colony formation assay with MDA-MB231 control and NCS1-OE cells. The assay was performed with 100, 200, and 500 initial cells, and the plot shows the percentage area covered at the end of the experiment as mean values ± 95% confidence intervals ($P < 0.01$ for all comparisons). *B*) Scratch assay demonstrating the wound healing capacity of NCS1-OE and control MDA-MB231 cells. The distance traveled (in pixels) was assessed after 24 h. Box plots represent $n = 3$ independent experiments per genotype. $^{**}P < 0.01$. *C*) Line plots showing the movement of MDA-MB231 control and NCS1-OE cells in collagen gels over a period of 8 h (in micrometers) as measured using time-lapse microscopy. Each colored trace represents an individual cell. *D, E*) Bar plots showing the MSD (μM^2) (*D*) and average velocity (μM/min) (*E*) of MDA-MB231 control and NCS1-OE cells in collagen gels over a period of 8 h. Values are means of $n = 40$ cells ± 95% confidence intervals ($P < 0.005$ and $P < 0.0001$, respectively).

Histopathologic assessment of lung specimens confirms the presence of multiple tumor cell clusters in the NCS1$^+$ group and small numbers of single tumor cells in the control

During the aforementioned mouse study (**Fig. 5*A***), mouse lungs were harvested after d 3 and 7, and again at the end of the study. Because the biggest differences between NCS1$^+$ and control tumors were found in the early phase (defined as the first 7 d) of tumor development, histopathologic assessment was conducted with a focus on these early tumors.

Lung tissue collected 7 d after tumor cell injection showed only a rare appearance of cancer cells in the lung specimens isolated from control mice and stained with H&E (Fig. 5*A* and Supplemental Table S2). Only 3 of the 8 control mouse lungs were found to contain a few single tumor cells (Supplemental Fig. S7 and Supplemental Table S2), whereas all lungs from NCS1$^+$ mice harbored tumor cells and 6 of these 8 lungs contained multiple clusters of tumor cells (Fig. 5*B, C* and Supplemental Table S2). Anti-NCS1 immunohistochemistry (IHC) staining was used to validate the expression of NCS1 in the cells that were identified as cancer cells in the H&E-stained slides (inset in Fig. 5C and Supplemental Table S3). These results indicate that overexpression of NCS1 causes a higher early incidence of metastasis in mouse lungs after tail-vein injection with a tumor cell suspension. This can be explained by an increase of the number of cells which survived to form colonies in the lung tissue or an increase of cell invasiveness upon NCS1 overexpression.

NCS1 overexpression confers a long-term survival advantage to tumor cells

Mouse lung specimens that were obtained at the end of the study were stained with H&E and inspected to investigate

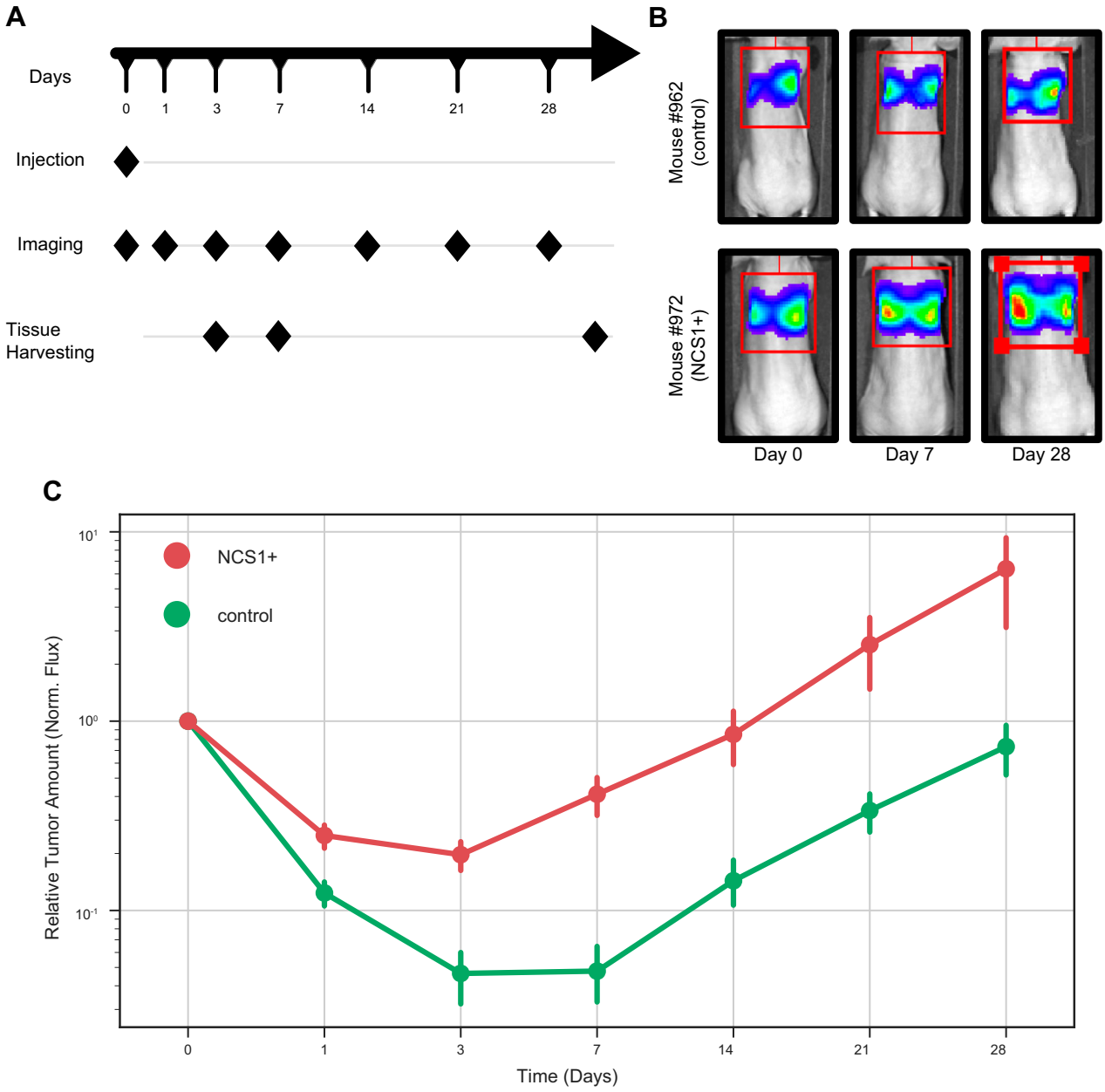

Figure 4. Mouse xenograft experiments show larger lung tumors from NCS1+-containing cells when compared with the control. *A*) Workflow schematic; $n = 16$ mice per group were injected *via* the tail vein with MDA-MB231 breast cancer cells overexpressing either NCS1 or a control vector. Lung tissue of 4 mice per group was harvested after 3 and 7 d and all mice were euthanized at the end of the study after d 28. Imaging studies measuring the photon flux of a luciferase reporter was performed on d 1, 3, 7, 14, 21, and 28. *B*) The panels show representative mouse images of a control mouse (962) and an NCS1$^+$ mouse (972). The color-coded luminescence signal indicates the relative amount of tumor in the mouse lungs with blue being a weak signal and red being a strong signal. *C*) Line plot showing the relative luminescence signal after normalization at each imaging time point. Until d 7, the fluorescence measurements decreased less in NCS1$^+$ tumors (red line plot) than in control tumors (green line plot). All tumors grow at similar rates from d 7 onwards.

the question whether NCS1 plays a role in mature tumors as well. Because all mice were euthanized after the respective lung tumor reached a large, predetermined size (10^9 absolute flux as measured using the method described above), a homogeneous histologic appearance of NCS1$^+$ and control tumors was anticipated.

Contrary to our expectations, we found large areas of necrosis in the control tumors (**Fig. 6*A***), whereas no necrotic cells could be identified in 3 of the 4 specimens from NCS1$^+$ tumors (Fig. 6*B* and Supplemental Table S1). A fourth specimen exhibited limited amounts of necrotic material as opposed to the large areas of necrosis in the control tumors. Histologically, no difference with regard to the overall tumor volume was found between NCS1$^+$ and control lungs, most likely because all tumors had reached a size where the lungs were completely filled with tumor cells (Supplemental Fig. S8). The absence of tumor cell death in the context of NCS1 overexpression suggests that even in a larger tumor, high NCS1 levels confer a survival advantage. This may impact the reactivity of the

tumor to treatment by preserving more living cells in the tumor's core.

DISCUSSION

In this study, we examined the effects of increased levels of NCS1 on tumor cell migration and survival *in vitro* and *in vivo*. We have previously observed that high NCS1 expression was significantly associated with an unfavorable prognosis in 2 independent breast cancer cohorts (41) as well as 2 publicly available liver cancer cohorts (42). Interestingly, NCS1 levels were highly correlated with expression levels of LIMK1, an enzyme associated with regulation of cell motility (27), when examining RNA sequencing data of liver samples from the Cancer Genome Atlas (48) and the International Cancer Genome Consortium (49). LIMK1 is a key regulator of the actin cytoskeleton and its high expression was previously identified as a potential driver of invasion in a variety of tumors (28–30). Other components of physiologic Ca^{2+} signaling are also known to regulate physiologic cell movement as well as tumor cell motility (21, 22, 24). Thus, we hypothesized that high levels of NCS1 may confer enhanced metastatic capability on tumor cells.

To investigate the molecular effects of increased NCS1, this Ca^{2+}-binding protein was stably overexpressed in the MDA-MB231 breast cancer cell line. First, we validated (41) that high levels of NCS1 do not alter cellular proliferation rates using 2 cell based growth assays. Another hallmark of aggressive, metastatic tumor cells shown to be regulated by NCS1 is their motility, which would enhance a cell's ability to spread to distant organs within the body. Accordingly, we found that upon overexpression of NCS1, cells exhibited a profoundly different morphology. In particular, they were less rounded and displayed an increased number of large cellular protrusions. This phenotype is consistent with enhanced motility and the capacity to form colonies.

To further study the effects of NCS1 overexpression on tumor cell morphology, immunofluorescence imaging was performed. We found that NCS1 preferentially localizes to the leading edge of migrating cells. Although this effect was independent of absolute expression levels, we found more NCS1 at cellular protrusions in cells that highly overexpressed NCS1. This finding supports the hypothesis that NCS1 might facilitate the movement of cancer cells *via* regulation of local Ca^{2+} at cell extensions. The colocalization between NCS1 and actin, specifically at the leading edge, suggests that NCS1 assists in regulating the continuous turnover of the actin cytoskeleton necessary for cell migration to occur.

We performed 2-D colony formation and wound healing assays to confirm that this morphologic change is also accompanied by a functional change. Indeed, NCS1-OE cells were more motile compared with the controls. In an attempt to more closely mimic the physiologic 3-D

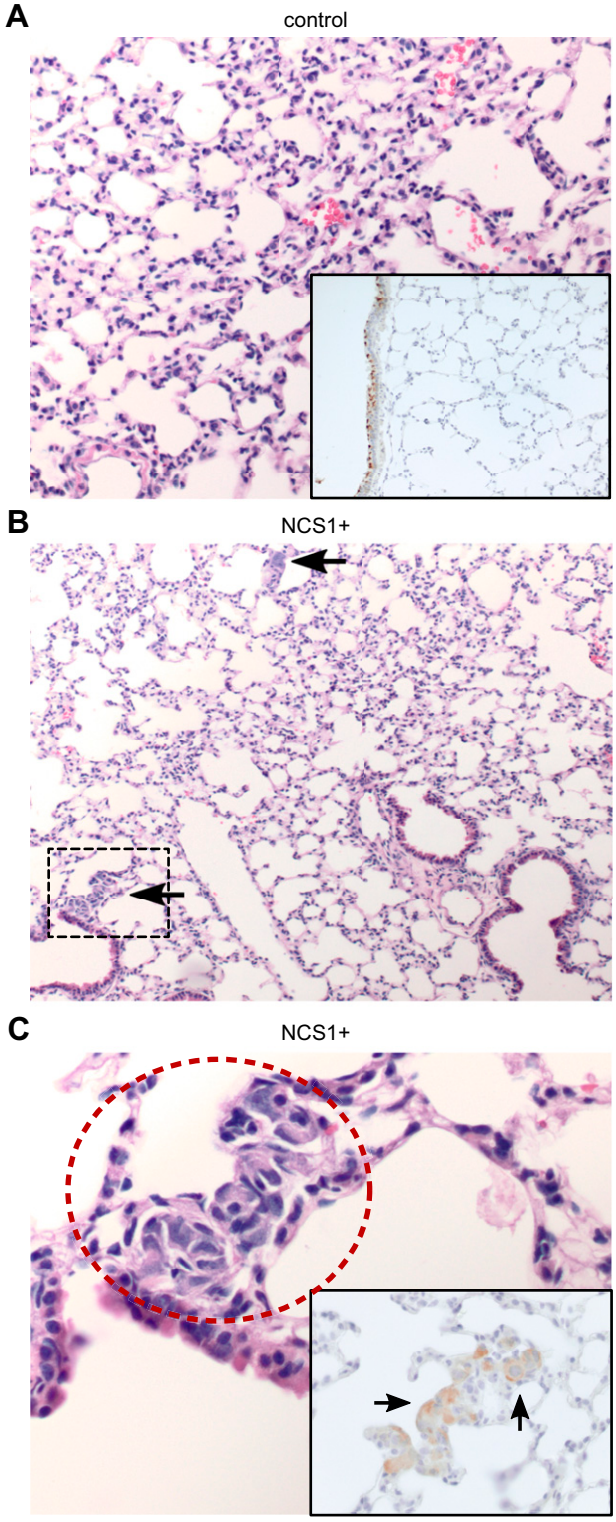

Figure 5. Lung specimens of NCS1+ mice contain large tumor cell clusters after 7 d. *A*) Tumor cells were not found in an H&E-stained lung specimen from a control mouse (966) that was euthanized after 7 d (medium magnification). Anti-NCS1 IHC staining confirms the absence of tumor cells (insert, high magnification). NCS1 staining within normal bronchial epithelium served as a positive control in all samples. *B*) Two prominent foci of tumor cells are visible (black arrows) in an H&E-stained lung specimen from an NCS1+ mouse (987) that was euthanized after 7 d (low magnification). *C*) High-magnification image of the region in *B* that is marked with a black box. Tumor cells are circled in red. The insert shows an anti-NCS1 IHC-stained specimen of mouse 987 (high magnification) demonstrating that the tumor cells were stained positively for NCS1 (black arrows).

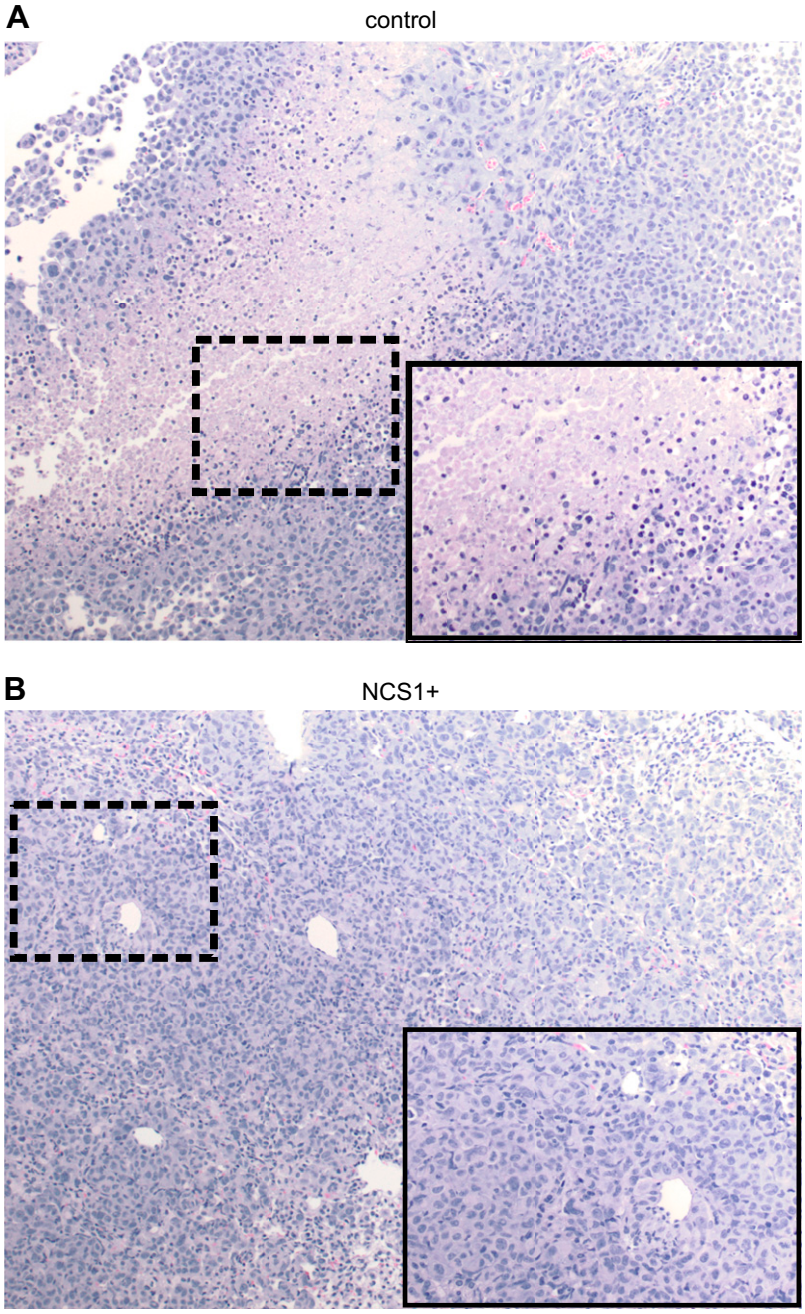

Figure 6. Lung specimens of NCS1$^+$ mice show no necrotic areas after more than 28 d of tumor growth. *A*) H&E-stained lung specimen (medium magnification) of a control mouse (952) at the end of the study. The insert shows an area of necrosis (black box) at high magnification. *B*) Picture of an H&E-stained lung specimen (medium magnification) of an NCS1$^+$ mouse (973) at the end of the study. Note the absence of necrotic cells. The insert shows a high magnification view of the area in the black box.

microenvironment in which cancers grow and to analyze the dynamics of MDA-MB231 cell movement *in vitro* (50, 51), we placed NCS1-OE and control cells in type I collagen gels and performed time-lapse microscopy to monitor their movement. Again, increased motility, as measured using the MSD and average speed, was observed.

Thus, the *in vitro* experiments performed in this study suggest that tumor cells that acquire high levels of NCS1 during tumorigenesis gain the advantage of being more motile. To explore the question of whether this *in vitro* phenotype also leads to an increased number of metastases *in vivo*, we used a mouse xenograft model. Engineered MDA-MB231 cells were injected into the tail vein of nude mice and a luciferase reporter was used to monitor tumor growth in the mouse lungs over time. Mice injected with high NCS1 levels presented with increased numbers of nascent tumors between d 0 and 7, but after this initial period, the growth rates of NCS1$^+$ and control tumors were similar. This finding in an intact mouse is in close alignment with our observations from *in vitro* experiments. If NCS1 impacted cell proliferation, we would have expected to see a difference in the overall tumor growth rates.

That NCS1 facilitates early tumor cell engraftment in the mouse lung suggests that NCS1 promotes cell survival as well as metastasis. In addition to examining mouse specimens at early time points during the experiment, specimens from larger tumors after more than 28 d were analyzed to gain more insight into how NCS1 overexpression impacts tumor behavior. Although all of the tumors were large, we observed differences between the groups. Control tumors presented with large necrotic

zones in all specimens, whereas NCS1$^+$ tumors did not. This difference indicates a survival advantage of cells with high NCS1 levels that extends beyond the initial metastatic expansion.

It is well known that major oncogenic pathways are regulated by cytoplasmic Ca^{2+}. Enhanced signaling *via* the PI3K/Akt pathway facilitates cell movement and increases cellular survival (52). NCS1 physically binds to PI4K (35, 36) and *via* this protein–protein interaction, it regulates the production of the second messenger molecule inositol 1,4,5 *tris*phosphate (53). InsP3 in turn activates the PI3K pathway. Furthermore, NCS1 interacts with InsP3Rs at the endoplasmic reticulum (ER) and upon binding, there is increased Ca^{2+} efflux from the ER (54). Previous research has shown that InsP3Rs are important contributors to an aggressive, prometastatic phenotype in cancer cells (21). The combination of these studies indicates that NCS1 enhances cell migration and survival *via* several routes. Upon overexpression, NCS1 binds to InsP3Rs and increases cytoplasmic Ca^{2+} concentrations. Ca^{2+} itself can act as a second messenger molecule and can facilitate cell movement. In addition, NCS1 may activate the PI3K pathway upon binding to PI4K.

Our previous study used 2 different breast cancer cell lines (MDA-MB231 and MCF-7), and similar responses to NCS1 overexpression were observed in both cell lines (41). In this study we focused on the triple-negative MDA-MB231 cells derived from plural effusion, as these cells are better able to metastasize to various organs (55). Various *in vitro* and *in vivo* experiments were performed to demonstrate the effects of NCS1 overexpression on several aspects of the cellular phenotype. In-depth mechanistic studies of the molecular effects of NCS1 are currently in preparation. Our future work will also reveal which parts of the Ca^{2+} signaling complex associated with NCS1 (42) are best suited for pharmacologic intervention.

CONCLUSIONS

This study demonstrates that overexpression of the Ca^{2+} binding protein NCS1 increases cellular motility and the invasive capacity of tumor cells *in vitro* and *in vivo* without altering growth rates. It lays the groundwork for studying the molecular mechanisms of NCS1- and Ca^{2+}-driven metastasis in cancers such as breast and liver tumors. Furthermore, it describes a set of experiments that can be used to test pharmacologic interventions to inhibit metastatic spread of tumor cells with high levels of NCS1. FJ

ACKNOWLEDGMENTS

The authors thank Dr. Sabine Lang (Yale University) for technical and administrative support. The authors acknowledge helpful discussions with Allison Brill, Dr. David Calderwood, and Dr. Tamar Taddei (Yale University). J.E.A., D.S., J.A.S., and H.K.G. received a scholarship from the German Academic Scholarship Foundation. M.Z. received a Brown Coxe Postdoctoral Fellowship from Yale University. W.L.C. received NSF Graduate Research Fellowship DGE-1122492. This work was supported, in part, by U.S. National Institutes of Health (NIH) National Institute of Diabetes and Digestive and Kidney Diseases Grant 5P01DK057751 (to B.E.E. and M.E.R.), NIH National Institute of Biomedical Imaging and Bioengineering (Grant 1R21EB026630 to M.M.), and U.S. Department of Defense Grant W81XWH-15-1-0117 (to Q.Y.). B.E.E. is a founder of Osmol Therapeutics, a company that is targeting NCS1 for therapeutic purposes. Primary data are maintained in the Ehrlich Laboratory at Yale University. Reagents not commercially available are available from the Ehrlich Laboratory. The authors declare no conflicts of interest.

AUTHOR CONTRIBUTIONS

J. E. Apasu, D. Schuette, and B. E. Ehrlich designed the study; J. E. Apasu, D. Schuette, R. LaRanger, J. A. Steinle, L. D. Nguyen, H. K. Grosshans, M. Zhang, and W. L. Cai contributed to experiments; M. E. Robert provided all pathology assessments; D. Schuette and B. E. Ehrlich wrote the first draft; and all authors edited the manuscript and have consented to publication.

REFERENCES

1. Hanahan, D., and Weinberg, R. A. (2011) Hallmarks of cancer: the next generation. *Cell* **144**, 646–674
2. Mehlen, P., and Puisieux, A. (2006) Metastasis: a question of life or death. *Nat. Rev. Cancer* **6**, 449–458
3. Taketo, M. M. (2011) Reflections on the spread of metastasis to cancer prevention. *Cancer Prev. Res. (Phila.)* **4**, 324–328
4. Lambert, A. W., Pattabiraman, D. R., and Weinberg, R. A. (2017) Emerging biological principles of metastasis. *Cell* **168**, 670–691
5. Berridge, M. J. (1993) Inositol trisphosphate and calcium signalling. *Nature* **361**, 315–325
6. Berridge, M. J. (1998) Neuronal calcium signaling. *Neuron* **21**, 13–26
7. Nguyen, T., Chin, W. C., and Verdugo, P. (1998) Role of Ca^{2+}/K^+ ion exchange in intracellular storage and release of Ca2+. *Nature* **395**, 908–912
8. Gunter, T. E., and Pfeiffer, D. R. (1990) Mechanisms by which mitochondria transport calcium. *Am. J. Physiol.* **258**, C755–C786
9. Berridge, M. J. (1995) Calcium signalling and cell proliferation. *BioEssays* **17**, 491–500
10. Smedler, E., and Uhlén, P. (2014) Frequency decoding of calcium oscillations. *Biochim. Biophys. Acta* **1840**, 964–969
11. Dolmetsch, R. E., Xu, K., and Lewis, R. S. (1998) Calcium oscillations increase the efficiency and specificity of gene expression. *Nature* **392**, 933–936
12. Clapham, D. E. (2007) Calcium signaling. *Cell* **131**, 1047–1058
13. Augustine, G. J., Santamaria, F., and Tanaka, K. (2003) Local calcium signaling in neurons. *Neuron* **40**, 331–346
14. Ghosh, A., and Greenberg, M. E. (1995) Calcium signaling in neurons: molecular mechanisms and cellular consequences. *Science* **268**, 239–247
15. Hajnóczky, G., Davies, E., and Madesh, M. (2003) Calcium signaling and apoptosis. *Biochem. Biophys. Res. Commun.* **304**, 445–454
16. Takemura, M., Mishima, T., Wang, Y., Kasahara, J., Fukunaga, K., Ohashi, K., and Mizuno, K. (2009) Ca^{2+}/calmodulin-dependent protein kinase IV-mediated LIM kinase activation is critical for calcium signal-induced neurite outgrowth. *J. Biol. Chem.* **284**, 28554–28562
17. Hanna, S., and El-Sibai, M. (2013) Signaling networks of Rho GTPases in cell motility. *Cell. Signal.* **25**, 1955–1961
18. Zheng, J. Q., and Poo, M. M. (2007) Calcium signaling in neuronal motility. *Annu. Rev. Cell Dev. Biol.* **23**, 375–404
19. Swaney, K. F., Huang, C.-H., and Devreotes, P. N. (2010) Eukaryotic chemotaxis: a network of signaling pathways controls motility, directional sensing, and polarity. *Annu. Rev. Biophys.* **39**, 265–289
20. Yi, M., Weaver, D., and Hajnóczky, G. (2004) Control of mitochondrial motility and distribution by the calcium signal: a homeostatic circuit. *J. Cell Biol.* **167**, 661–672
21. Ando, H., Kawaai, K., Bonneau, B., and Mikoshiba, K. (2018) Remodeling of Ca^{2+} signaling in cancer: regulation of inositol 1,4,5-trisphosphate receptors through oncogenes and tumor suppressors. *Adv. Biol. Regul.* **68**, 64–76

22. Florea, A. M., and Büsselberg, D. (2009) Anti-cancer drugs interfere with intracellular calcium signaling. *Neurotoxicology* **30**, 803–810
23. Chen, Y. F., Chen, Y. T., Chiu, W. T., and Shen, M. R. (2013) Remodeling of calcium signaling in tumor progression. *J. Biomed. Sci.* **20**, 23
24. Stewart, T. A., Yapa, K. T. D. S., and Monteith, G. R. (2015) Altered calcium signaling in cancer cells. *Biochim. Biophys. Acta* **1848**, 2502–2511
25. Xiao, M., Li, T., Ji, Y., Jiang, F., Ni, W., Zhu, J., Bao, B., Lu, C., and Ni, R. (2018) S100A11 promotes human pancreatic cancer PANC-1 cell proliferation and is involved in the PI3K/AKT signaling pathway. *Oncol. Lett.* **15**, 175–182
26. Gonzalez Guerrico, A. M., Jaffer, Z. M., Page, R. E., Braunewell, K. H., Chernoff, J., and Klein-Szanto, A. J. (2005) Visinin-like protein-1 is a potent inhibitor of cell adhesion and migration in squamous carcinoma cells. *Oncogene* **24**, 2307–2316
27. Prunier, C., Prudent, R., Kapur, R., Sadoul, K., and Lafanechère, L. (2017) LIM kinases: cofilin and beyond. *Oncotarget* **8**, 41749–41763
28. Scott, R. W., Hooper, S., Crighton, D., Li, A., König, I., Munro, J., Trivier, E., Wickman, G., Morin, P., Croft, D. R., Dawson, J., Machesky, L., Anderson, K. I., Sahai, E. A., and Olson, M. F. (2010) LIM kinases are required for invasive path generation by tumor and tumor-associated stromal cells. *J. Cell Biol.* **191**, 169–185
29. Scott, R. W., and Olson, M. F. (2007) LIM kinases: function, regulation and association with human disease. *J. Mol. Med. (Berl.)* **85**, 555–568
30. Li, R., Doherty, J., Antonipillai, J., Chen, S., Devlin, M., Visser, K., Baell, J., Street, I., Anderson, R. L., and Bernard, O. (2013) LIM kinase inhibition reduces breast cancer growth and invasiveness but systemic inhibition does not reduce metastasis in mice. *Clin. Exp. Metastasis* **30**, 483–495
31. Boeckel, G. R., and Ehrlich, B. E. (2018) NCS-1 is a regulator of calcium signaling in health and disease. *Biochim. Biophys. Acta. Mol. Cell Res.* **1865**, 1660–1667
32. Weiss, J. L., Hui, H., and Burgoyne, R. D. (2010) Neuronal calcium sensor-1 regulation of calcium channels, secretion, and neuronal outgrowth. *Cell. Mol. Neurobiol.* **30**, 1283–1292
33. D'Onofrio, S., Kezunovic, N., Hyde, J. R., Luster, B., Messias, E., Urbano, F. J., and Garcia-Rill, E. (2015) Modulation of gamma oscillations in the pedunculopontine nucleus by neuronal calcium sensor protein-1: relevance to schizophrenia and bipolar disorder. *J. Neurophysiol.* **113**, 709–719
34. Burgoyne, R. D., and Weiss, J. L. (2001) The neuronal calcium sensor family of Ca^{2+}-binding proteins. *Biochem. J.* **353**, 1–12
35. Rajebhosale, M., Greenwood, S., Vidugiriene, J., Jeromin, A., and Hilfiker, S. (2003) Phosphatidylinositol 4-OH kinase is a downstream target of neuronal calcium sensor-1 in enhancing exocytosis in neuroendocrine cells. *J. Biol. Chem.* **278**, 6075–6084
36. Haynes, L. P., Fitzgerald, D. J., Wareing, B., O'Callaghan, D. W., Morgan, A., and Burgoyne, R. D. (2006) Analysis of the interacting partners of the neuronal calcium-binding proteins L-CaBP1, hippocalcin, NCS-1 and neurocalcin δ. *Proteomics* **6**, 1822–1832
37. Blasiole, B., Kabbani, N., Boehmler, W., Thisse, B., Thisse, C., Canfield, V., and Levenson, R. (2005) Neuronal calcium sensor-1 gene ncs-1a is essential for semicircular canal formation in zebrafish inner ear. *J. Neurobiol.* **64**, 285–297
38. Koizumi, S., Rosa, P., Willars, G. B., Challiss, R. A., Taverna, E., Francolini, M., Bootman, M. D., Lipp, P., Inoue, K., Roder, J., and Jeromin, A. (2002) Mechanisms underlying the neuronal calcium sensor-1–evoked enhancement of exocytosis in PC12 cells. *J. Biol. Chem.* **277**, 30315–30324
39. Choe, C. U., and Ehrlich, B. E. (2006) The inositol 1,4,5-trisphosphate receptor (IP3R) and its regulators: sometimes good and sometimes bad teamwork. *Sci. STKE* **2006**, re15
40. Boehmerle, W., Splittgerber, U., Lazarus, M. B., McKenzie, K. M., Johnston, D. G., Austin, D. J., and Ehrlich, B. E. (2006) Paclitaxel induces calcium oscillations via an inositol 1,4,5-trisphosphate receptor and neuronal calcium sensor 1-dependent mechanism. *Proc. Natl. Acad. Sci. USA* **103**, 18356–18361
41. Moore, L. M., England, A., Ehrlich, B. E., and Rimm, D. L. (2017) Calcium sensor, NCS-1, promotes tumor aggressiveness and predicts patient survival. *Mol. Cancer Res.* **15**, 942–952
42. Schuette, D., Moore, L. M., Robert, M. E., Taddei, T. H., and Ehrlich, B. E. (2018) Hepatocellular carcinoma outcome is predicted by expression of neuronal calcium sensor 1. *Cancer Epidemiol. Biomarkers Prev.* **27**, 1091–1100
43. Guzmán, C., Bagga, M., Kaur, A., Westermarck, J., and Abankwa, D. (2014) ColonyArea: an ImageJ plugin to automatically quantify colony formation in clonogenic assays. *PLoS One* **9**, e92444
44. Livak, K. J., and Schmittgen, T. D. (2001) Analysis of relative gene expression data using real-time quantitative PCR and the $2^{-\Delta\Delta C_T}$ method. *Methods* **25**, 402–408
45. Ponomarev, V., Doubrovin, M., Serganova, I., Vider, J., Shavrin, A., Beresten, T., Ivanova, A., Ageyeva, L., Tourkova, V., Balatoni, J., Bornmann, W., Blasberg, R., and Gelovani Tjuvajev, J. (2004) A novel triple-modality reporter gene for whole-body fluorescent, bioluminescent, and nuclear noninvasive imaging. *Eur. J. Nucl. Med. Mol. Imaging.* **31**, 740–751
46. Stuelten, C. H., Parent, C. A., and Montell, D. J. (2018) Cell motility in cancer invasion and metastasis: insights from simple model organisms. *Nat. Rev. Cancer* **18**, 296–312
47. Friedl, P., and Gilmour, D. (2009) Collective cell migration in morphogenesis, regeneration and cancer. *Nat. Rev. Mol. Cell Biol.* **10**, 445–457
48. Cancer Genome Atlas Research Network. (2017) Comprehensive and integrative genomic characterization of hepatocellular carcinoma. *Cell* **169**, 1327–1341.e23
49. Fujimoto, A., Furuta, M., Totoki, Y., Tsunoda, T., Kato, M., Shiraishi, Y., Tanaka, H., Taniguchi, H., Kawakami, Y., Ueno, M., Gotoh, K., Ariizumi, S., Wardell, C. P., Hayami, S., Nakamura, T., Aikata, H., Arihiro, K., Boroevich, K. A., Abe, T., Nakano, K., Maejima, K., Sasaki-Oku, A., Ohsawa, A., Shibuya, T., Nakamura, H., Hama, N., Hosoda, F., Arai, Y., Ohashi, S., Urushidate, T., Nagae, G., Yamamoto, S., Ueda, H., Tatsuno, K., Ojima, H., Hiraoka, N., Okusaka, T., Kubo, M., Marubashi, S., Yamada, T., Hirano, S., Yamamoto, M., Ohdan, H., Shimada, K., Ishikawa, O., Yamaue, H., Chayama, K., Miyano, S., Aburatani, H., Shibata, T., and Nakagawa, H. (2016) Whole-genome mutational landscape and characterization of noncoding and structural mutations in liver cancer. *Nat. Genet.* **48**, 500–509
50. Riching, K. M., Cox, B. L., Salick, M. R., Pehlke, C., Riching, A. S., Ponik, S. M., Bass, B. R., Crone, W. C., Jiang, Y., Weaver, A. M., Eliceiri, K. W., and Keely, P. J. (2014) 3D collagen alignment limits protrusions to enhance breast cancer cell persistence. *Biophys. J.* **107**, 2546–2558
51. Wu, P.-H., Giri, A., Sun, S. X., and Wirtz, D. (2014) Three-dimensional cell migration does not follow a random walk. *Proc. Natl. Acad. Sci. USA* **111**, 3949–3954
52. Vivanco, I., and Sawyers, C. L. (2002) The phosphatidylinositol 3-kinase AKT pathway in human cancer. *Nat. Rev. Cancer* **2**, 489–501
53. Balla, A., and Balla, T. (2006) Phosphatidylinositol 4-kinases: old enzymes with emerging functions. *Trends Cell Biol.* **16**, 351–361
54. Schlecker, C., Boehmerle, W., Jeromin, A., DeGray, B., Varshney, A., Sharma, Y., Szigeti-Buck, K., and Ehrlich, B. E. (2006) Neuronal calcium sensor-1 enhancement of InsP3 receptor activity is inhibited by therapeutic levels of lithium. *J. Clin. Invest.* **116**, 1668–1674
55. Fantozzi, A., and Christofori, G. (2006) Mouse models of breast cancer metastasis. *Breast Cancer Res.* **8**, 212

Received for publication September 18, 2018.
Accepted for publication December 3, 2018.